FLEXIBILITY EXPLOITATION FOR RESIDENTIAL, TERTIARY AND INDUSTRIAL BUILDINGS

FLEXBIT PROJECT

CETPartnership Joint Call 2023

D2.1 Development Report on Energy Exchange Mechanisms

Lead Author: Next Multiservice / Francesco Saverio Cannizzaro orcid: https://orcid.org/0009-0004-1528-1682

Contributed authors:
Pio Alessandro Lombardi orcid: https://orcid.org/0000-0003-4598-9759
Gaetano Zizzo orcid: https://orcid.org/0000-0003-4413-4855
Mateusz Witkowski orcid: https://orcid.org/0009-0005-4439-1458
Szymon Smagowski orcid: https://orcid.org/0009-0003-1965-8099
Lorenzo Bartolucci orcid: https://orcid.org/0000-0003-4258-4860
Finn Bennet Schröder orcid: [missing]
Christina Karatrantou orcid: https://orcid.org/0009-0008-9818-048X
Pavlos Tyrologou orcid: https://orcid.org/0000-0001-7706-1774
Muhammad Mahad Malik orcid: [missing]
Alessandro Polimeni orcid: https://orcid.org/0009-0005-9359-8746
Tomasz Sikorski orcid: https://orcid.org/0000-0002-4423-7216
Jacek Rezmer orcid: https://orcid.org/0000-0002-2822-7595
Vishnu Suresh orcid: https://orcid.org/0000-0003-2891-9206
Marek Kott orcid: https://orcid.org/0000-0001-9865-4675
Tomasz Okoń orcid: https://orcid.org/0000-0003-3651-5666
Lukasz Michalec orcid: https://orcid.org/0000-0002-2192-833X
Anna Pawlica orcid: https://orcid.org/0000-0002-4975-1804
Dominika Kaczorowska orcid: : https://orcid.org/0000-0002-2312-2903

DOI **10.5281/zenodo.20505332**

This research was funded by CETPartnership, the Clean Energy Transition Partnership under the 2023 joint call for research proposals, co-funded by the European Commission (GA N°101069750) and with the funding organizations detailed on https://cetpartnership.eu/funding-agencies-and-call-modules.

Co-funded by the European Union

Supported by:

Federal Ministry for Economic Affairs and Climate Action

on the basis of a decision by the German Bundestag

FlexBIT Consortium

Table of Contents

1 Executive summary

1.1 Purpose

This deliverable serves as the primary reference document for the development status of the **FlexBIT energy exchange mechanisms** and the associated **enabling platform**, developed within the framework of **Work Package 2 (WP2)** activities.

The main objective of this document is to provide a comprehensive overview that progresses from conceptual models to **functional design** and the definition of the **technical architecture**. The latter focuses on establishing standardized data exchange protocols and **APIs**, which are essential elements for ensuring the implementation and operational functionality of these mechanisms across an ecosystem of **heterogeneous demonstrators**, each characterized by diverse hardware configurations and application contexts.

1.2 Scope and data coverage

Section 1.2 defines the operational perimeter of the document, specifying the data and interfaces required to enable energy exchange scenarios across the various FlexBIT pilot sites. Data coverage is structured around four fundamental pillars:

- Operational Data Streams (IoT and Energy): The FlexBIT platform relies on operational measurements acquired at pilot sites through local adapters. Rather than receiving raw real-time telemetry directly at platform level, these adapters collect data from local devices and systems and transmit them as aggregated metrics over a defined time interval, typically 15 minutes. Covered variables include, where applicable, PV generation, site electric demand, Battery Energy Storage Systems (BESS) power and state of charge, EVSE/V2G charging sessions, and other site-specific energy vectors such as thermal (heat and cool), hydrogen, or compressed air-related measurements.
- Standardization and Interoperability: To ensure comparability across heterogeneous demonstrators, the exchanged data is accompanied by standardized metadata, including units of measure, timestamps and time zones, device identifiers, and quality flags. The detailed data model, canonical fields, interoperability requirements, and exchange specifications are defined in Deliverable D2.3.
- Contextual Inputs for System Intelligence: In addition to site measurements, the platform may use external contextual inputs required by forecasting and optimization functions, such as weather data and energy market price signals, in line with the project architecture and objectives [2].
- Temporal Resolution and Dynamics: Platform-level forecasting, optimization, and coordination are based on standardized time intervals, typically 15 minutes, however, in the case of local applications, shorter intervals such as 1, 5, 10 minutes are considered. This reflects the adopted data exchange model, in which local adapters preprocess and aggregate site-level measurements before transmitting them to the centralized platform. For sky forecasting optimization case, described in detail in Deliverable D2.2, the interval for sky-image analysis is fixed to 1 minute.

2 Introduction and Objectives

2.1 Background and motivation

The increasing penetration of non-programmable Renewable Energy Sources (RES) is changing the operation of electricity systems at building, community, and grid level. While photovoltaic and other volatile renewable sources are essential for decarbonization, their variability creates new balancing needs, local congestion risks [2, 3], and stronger requirements for coordination between generation, storage, and demand. In low-voltage networks, these challenges often appear as voltage rise issues associated with high local PV penetration, requiring coordinated management of distributed generation, including the use of inverter-based active and reactive power capabilities to maintain voltage within acceptable limits while reducing unnecessary curtailment. These challenges are further intensified by the electrification of transport and heating, which can increase load peaks and stress existing network assets. FlexBIT is positioned in this context, with the objective of enabling a cost-efficient, secure, and resilient integration of high shares of volatile RES, up to scenarios approaching 100% renewable penetration.

To address these challenges, FlexBIT develops a **digital platform** able to **aggregate distributed flexible resources** of different types and orchestrate their contribution to several energy services. In the project vision, buildings and local energy systems are not treated as passive consumers, but as active nodes that can generate, dynamically consume, store, exchange, and flexibly manage energy [1, 4]. This includes support for **self-consumption optimization** within Renewable Energy Communities (RECs), balancing and congestion resolution, and the coordinated exploitation of local flexibility across residential, tertiary, and industrial contexts. The project also emphasizes the use of **AI-based forecasting**, **data-driven control**, and secure data exchange to identify the most suitable flexibility options and user clusters for each service.

Further motivation for FlexBIT is the need to integrate heterogeneous technologies and energy vectors within a common interoperable framework. The project therefore combines electrical assets with other flexibility-enabling resources, including batteries, hydrogen systems, thermal storage, EV/V2G infrastructure, controllable loads, and compressed air. This multi-vector and multi-site perspective is reflected in the seven demonstrators, which cover different technical and operational contexts, from industrial communities and smart parking systems to hydrogen laboratories, solar cooling, and digital twin microgrids.

In practical terms, the project addresses four closely related needs:

- **integration** of distributed renewable generation without compromising local reliability;
- **exploitation** of hidden flexibility in buildings, storage systems, and controllable loads;
- **interoperability** between heterogeneous local systems and a common digital platform;
- **secure and traceable coordination** of energy exchange, optimization, and settlement processes.

2.2 Objectives of this deliverable

This deliverable defines the development framework for the FlexBIT energy exchange mechanisms within Work Package 2. Its role is to translate the project goals and architectural principles into a coherent functional structure that can be applied across the demonstrators. In this sense, the document does not only describe general concepts, but identifies the mechanisms, scenarios, and integration assumptions needed to support practical implementation.

More specifically, D2.1 pursues the following objectives:

1. Define the operational logic of energy exchange mechanisms: the deliverable describes how the main FlexBIT scenarios are structured, including self-consumption and community sharing, flexibility activation, local balancing, ancillary-service-oriented applications where relevant and it also considers the coordinated control of distributed generation units, particularly photovoltaic inverters, to support

voltage regulation and maximize renewable energy utilization through the optimal use of their active and reactive power capabilities. It clarifies the functional roles of measurements, allocation logic, dispatch generation, monitoring, and accounting [1, 2].

2. **Provide the functional framework for cross-demonstrator implementation**: the deliverable establishes a common functional reference for the development of energy exchange mechanisms across heterogeneous demonstrators. Rather than detailing interoperability specifications, it identifies the main asset categories, interaction logic, and platform-level functional assumptions that must be consistently considered across pilot implementations. The detailed data models, exchange specifications, and interoperability requirements are addressed in Deliverable D2.3.
3. **Document the integration model between local sites and the central platform**: the deliverable formalizes how pilot sites interact with the FlexBIT platform through adaptation layers and platform interfaces, while preserving local operational autonomy. This includes the distinction between local control responsibilities and centralized supervisory or advisory functions.
4. **Support the implementation and validation activities of WP2 and WP3**: by structuring the main mechanisms and defining minimum functional expectations, D2.1 provides a reference for subsequent implementation, demonstrator onboarding, and site-specific validation.

2.3 Inputs and alignment

This deliverable is developed in alignment with the overall FlexBIT project framework and with the architectural principles defined in Deliverable D1.1. It builds on the FlexBIT Architecture Blueprint, which describes the platform as a modular and layered ecosystem integrating distributed energy resources, IoT infrastructures, SCADA systems, analytics modules, and market-facing interfaces within a secure, scalable, and interoperable environment.

Within this framework, D2.1 focuses specifically on the energy exchange mechanisms and their functional implementation. The adopted approach is intended to ensure consistency with the project architecture while supporting scalability across heterogeneous demonstrators and maintaining a high level of cybersecurity. This alignment is not limited to technical coherence but also reflects the regulatory context in which the project operates, including cybersecurity obligations and legal requirements related to data exchange in the energy sector [1].

2.4 Architecture Reference

The overall FlexBIT architecture, as defined in Deliverable D1.1, is based on a modular and layered structure designed to integrate physical energy assets and digital services within a common framework. This architecture brings together distributed energy resources, IoT infrastructures, SCADA and EMS environments, data acquisition and processing components, forecasting and optimization modules, as well as platform interfaces for monitoring, coordination, and market-oriented services. Its purpose is to ensure that heterogeneous technologies can operate within a secure, scalable, and interoperable ecosystem across all demonstrators.

A key architectural principle of FlexBIT is the combination of local autonomy and central coordination. [4] The platform is not designed to replace local control systems, but to complement them through a supervisory layer capable of processing aggregated operational and contextual information and generating optimization-oriented recommendations. In this way, FlexBIT supports coordinated decision-making across different sites while preserving the technical independence and safety requirements of each demonstrator.

This concept is implemented through a two-loop control model:

1. **Fast Local Control Loop:** this loop is managed directly at **pilot-site level** through local automation systems such as SCADA, PLC, or EMS platforms. It is responsible for real-time plant operation, including equipment control, safety responses, battery charge/discharge actions, inverter control, and other site-specific technical functions. **Operating on timescales from milliseconds to seconds**, this layer ensures operational reliability and responsiveness without depending on continuous external coordination.

2. **Slow Advisory Loop**: this loop is coordinated by the centralized FlexBIT platform. It receives aggregated operational and contextual data from the demonstrators through platform interfaces such as **OpenAPI** or **Kakfa streams**, and processes them through forecasting, analytics, and flexibility optimization functions. On this basis, **the platform generates advisory signals, schedules, or coordination recommendations**, for example to improve self-consumption, optimize storage dispatch, support balancing and flexibility services and include optimized setpoints for distributed resources, such as photovoltaic inverters, where active and reactive power are jointly adjusted to mitigate voltage constraints and improve overall system efficiency . This layer operates on slower timescales, typically from minutes to hours, and does not interfere with the local safety and real-time control logic of the pilot sites.

The communication framework underlying this architecture is equally important. D1.1 identifies a **set of standard protocols and interfaces** used across the project, including Modbus TCP, IEC 61850, OPC UA, MQTT, and REST APIs over HTTPS, w
ured through TLS. This protocol diversity reflects the heterogeneity of the demonstrators, while the platform architecture provides a common integration approach capable of harmonizing different local implementations.

Finally, the relevance of **this architecture is reinforced by the diversity of the FlexBIT pilot environments**, which include industrial energy communities, hydrogen-based laboratory systems, smart parking with V2G, solar cooling applications, digital twin microgrids, and industrial EMS-based demonstrators. The modular and layered design is therefore essential not only for technical integration, but also for ensuring that common energy exchange mechanisms can be implemented across pilots with different assets, control systems, and flexibility objectives.

3 Energy Exchange Concept in FlexBIT

3.1 Definition of Energy Exchange Mechanisms

Energy exchange mechanisms in FlexBIT are the operational rules and workflows enabling: (i) **self-consumption and community sharing**, (ii) **flexibility activation** to support grid/community objectives, and (iii) **local balancing / ancillary services** where legally and technically feasible.

3.2 Operational Scenarios (REC, Flexibility, Balancing)

Scenarios covered in this deliverable:

- **REC self-consumption & sharing** (community allocation and accounting)
- **Flexibility activation** (demand response, load shifting, storage dispatch, and coordinated control of distributed generation through active and reactive power)
- **Balancing / ancillary services** (site-specific; depends on jurisdiction and telemetry/response requirements)

Jurisdiction note: REC rules differ by country; partners must describe the local regulatory assumptions used for their demonstrator (D1.2 provides the baseline context by country).

3.3 Role of Prosumers, Aggregators, and Communities

Energy exchange mechanisms require clear allocation of responsibilities between the actors involved in measurement acquisition, flexibility provision, coordination, and supervisory decision-making. In this context, the overall operational structure involves local energy assets, community-level coordination entities, and centralized platforms responsible for forecasting, optimization, and service orchestration. This division of roles enables coordinated flexibility management while preserving local technical autonomy and compliance with operational constraints.

Figure 3.1 System Architecture Overview: Multi-Layer Energy Exchange Ecosystem

3.3.1 Prosumer / Site Layer

The lowest operational level relies on prosumers or local sites as the physical source of energy production, consumption, and flexibility provision. These actors represent residential, tertiary, or industrial energy nodes

equipped with Distributed Energy Resources (DERs), including photovoltaic systems, battery energy storage systems (BESS), electric vehicle charging infrastructure, heat pumps, HVAC systems, and controllable electrical loads.
The primary responsibility of this layer is the generation of operational measurements. These include active and reactive power measurements, voltage and current values, battery state of charge, EV charging status, thermal conditions, and other locally relevant telemetry. Such measurements constitute the fundamental input for higher-level forecasting and optimization processes.
In addition to measurement provision, prosumer sites expose controllable flexibility resources to the FlexBIT ecosystem. However, this flexibility is not unconditional. Local Energy Management Systems (LEMS), SCADA platforms, or equivalent control infrastructure validate all external dispatch requests against site-specific constraints, including:

- inverter operating limits,
- battery charging/discharging boundaries,
- EV user mobility constraints,
- thermal comfort boundaries,
- equipment protection requirements,
- contractual or operational restrictions.

As a result, the site layer acts not only as a flexibility provider but also as a local constraint enforcement mechanism. This ensures that maintains principle of preserving local autonomy while enabling coordinated participation in broader flexibility services.

3.3.2 Community Operator Layer

Above the individual prosumer level, the community operator provides coordination logic for local energy sharing and collective flexibility participation. This role is particularly relevant in Renewable Energy Communities (RECs), Citizen Energy Communities (CECs), or other collective self-consumption structures.
The community operator does not directly control physical assets. Instead, its primary function is to define the operational rules governing energy exchange within the local community. Its responsibilities include:

- defining energy sharing windows,
- establishing allocation priorities among participants,
- specifying governance and participation rules,
- maintaining accounting and settlement logic,
- managing internal balancing assumptions,
- coordinating community-level flexibility participation.

Allocation windows determine when locally generated renewable energy may be shared between members. Allocation logic defines how this shared energy is distributed, for example according to proportional allocation, contractual priorities, fairness policies, or economic optimization rules.
Accounting logic ensures traceability of energy exchanges and supports settlement processes required for regulatory compliance or internal cost allocation.
The community operator therefore acts as the organizational coordination layer between individual technical assets and higher-level optimization services.

Figure 3.2 Community Operator Layer: Sharing Logic, Allocation, and Accounting

3.3.3 Platform / Aggregator Layer

The platform or aggregator layer constitutes the computational intelligence of the FlexBIT architecture. This layer aggregates measurements and contextual information from multiple sites and converts them into optimization-oriented operational recommendations.
Its main responsibilities include:

- telemetry aggregation,
- data validation and preprocessing,
- forecasting of renewable generation and load,
- uncertainty modelling,
- congestion-aware optimization,
- cost optimization,
- flexibility scheduling,
- advisory dispatch generation,
- execution supervision,
- coordination with external market or grid actors.

The forecasting engine processes multiple data streams, including:

- site telemetry,
- PV inverter data,
- battery SOC measurements,
- EV charging states,

- thermal demand indicators,
- weather forecasts,
- tariff or market signals.

Based on these inputs, the optimization engine calculates recommended operating strategies that satisfy multiple objectives simultaneously, such as:

- maximizing self-consumption,
- reducing network congestion,
- minimizing operational cost,
- preserving user comfort,
- increasing renewable hosting capacity,
- enabling participation in flexibility services.

The resulting dispatch remains advisory in nature. Real-time execution authority remains at local site level, where commands are validated against operational constraints before implementation.
The aggregator layer additionally supervises execution by comparing planned versus delivered flexibility, verifying response quality, and providing operational reporting.

Figure 3.3 Platform / Aggregator Intelligence Layer

The execution of flexibility services follows a structured operational workflow that transforms distributed measurements into coordinated flexibility actions. This workflow reflects the separation of responsibilities between local assets, supervisory intelligence, and external grid actors.

The process begins with real-time measurement acquisition at the prosumer or site level. Local monitoring infrastructure collects operational parameters such as active and reactive power, voltage, current, battery state of charge, EV charging status, thermal measurements, and community coordination signals. These measurements provide the operational visibility required for flexibility assessment.

The second step involves data validation and preprocessing. Before being used by supervisory applications, telemetry is checked for completeness, timestamp consistency, outlier detection, and communication integrity. This stage ensures that forecasting and optimization functions rely on reliable operational data.

Based on validated measurements and contextual information, the platform performs forecasting of relevant operational variables, including photovoltaic generation, site demand, battery availability, EV charging needs, and uncertainty margins. Forecasting provides the predictive layer required for proactive rather than purely reactive flexibility coordination.

The next stage is optimization, where the platform determines the most suitable flexibility actions while considering multiple objectives such as congestion mitigation, cost reduction, renewable energy maximization, and compliance with technical constraints. Optimization may involve coordinated scheduling of storage systems, demand response actions, EV charging management, or distributed generation control.

The result of this process is the generation of an advisory dispatch plan, which defines recommended control actions for participating resources. These actions may include active power modulation, battery scheduling, EV charging adjustments, thermal load control, or reactive power support.

Before implementation, dispatch actions undergo local validation at the site level. Local EMS or equivalent control systems verify that the requested actions comply with equipment limits, user comfort boundaries, battery operating constraints, inverter protection settings, and site-specific technical restrictions.

Once validated, the actions proceed to execution, performed by local control infrastructure such as EMS platforms, inverter controllers, battery management systems, or EV charging systems.

Finally, the process concludes with verification and accounting, where the delivered flexibility is measured, validated against the requested response, and recorded for settlement, reporting, and compliance purposes.

This operational workflow provides the practical execution logic underlying the proposed flexibility coordination architecture.

Table 3.1 ***Operational Workflow***

STEP	**FUNCTION / DESCRIPTION**
1. MEASUREMENTS	Real-time collection of: active/reactive power; voltage/current, battery SOC; EV charging state; thermal measurements; community allocation signals
2. DATA VALIDATION	Quality assurance: missing data detection; outlier filtering; timestamp consistency; telemetry integrity verification
3. FORECASTING	Prediction of: PV generation; flexible demand; storage availability; EV charging demand; uncertainty envelopes
4. OPTIMIZATION	Optimization objectives: Congestion mitigation; cost minimization; flexibility scheduling; DER coordination; local constraint compliance
5. ADVISORY DISPATCH GENERATION	Dispatch actions: active power modulation; reactive support; storage scheduling; EV charging orchestration; thermal load control

6. LOCAL VALIDATION	Constraint enforcement at prosumer/site level: inverter limits; voltage limits; SOC constraints; comfort boundaries
7. EXECUTION	Dispatch execution by: local EMS; inverter controllers; battery controllers; EV charging systems
8. VERIFICATION AND ACCOUNTING	delivery verification; settlement calculation; community accounting; compliance reporting

3.3.4 Example of Practical Flexibility Service (TAURON Distribution Model)

A practical example of a flexibility service within the FlexBIT operational context is provided by the flexibility service model introduced by TAURON Dystrybucja, one of the first Distribution System Operators in Poland implementing structured flexibility procurement mechanisms. These services are intended to improve distribution network reliability by using controllable distributed resources as an operational alternative to conventional grid reinforcement.
The primary objective of such services is congestion management and operational support of the distribution network. With increasing penetration of distributed renewable generation, especially photovoltaic systems, DSOs face technical challenges including transformer overload, feeder congestion, voltage rise, temporary power quality violations, and limited renewable hosting capacity.
Instead of relying exclusively on infrastructure expansion, flexibility services allow temporary operational adjustments by connected participants. These actions may include:

- temporary reduction of electricity consumption,
- shifting demand to periods of renewable surplus,
- battery charging or discharging,
- EV charging modulation,
- temporary generation curtailment.

In this service model, the DSO defines the technical flexibility requirement, including activation conditions, required response magnitude, and service duration. Flexibility providers or aggregators coordinate distributed assets by collecting telemetry, forecasting available flexibility, optimizing response strategies, and supervising execution.
Participating local assets may include industrial consumers, commercial buildings, battery systems, EV charging infrastructure, and prosumer installations equipped with controllable resources. Final execution remains subject to local technical constraints and operational feasibility. A typical operational sequence includes:

1. identification of a grid constraint requiring intervention;
2. specification of the required flexibility service;
3. aggregation and forecasting of available flexible resources;
4. optimization of the response strategy;
5. local validation of requested actions;
6. execution through local control systems;
7. verification of delivered flexibility;
8. settlement and accounting.

This example demonstrates how flexibility services can be implemented in practice using the general principles of measurement acquisition, supervisory optimization, local validation, and controlled execution.

3.4 Vehicle-to-grid (V2G) integration solutions to support electric vehicles

3.4.1 Introduction

The rise of EVs represents a crucial step in the strategy to reduce greenhouse gas emissions linked to global warming. The automotive market has evolved significantly in recent years; in fact, out of a total of approximately 1.47 billion

cars on the road worldwide today, about 40 million are electric, accounting for 2.7% of the global vehicle fleet [7]. The growing development of the EV market in Europe is a key element in making European countries climate-neutral by 2050. To achieve this goal, the European Commission has adopted the "Fit for 55" package to reduce vehicle emissions by 55% by 2030 and bring emissions from new cars to zero by 2035 [8]. EVs are an important tool for achieving Europe's goals, but their impact on the power grid must not be overlooked [9], [10]. In fact, it has been observed that charging EVs can cause power quality issues, such as voltage sags, current and voltage harmonics, and power imbalances [11].

In addition, EV charging during peak load periods can lead to increased energy demand and a greater need for generation capacity [12]. These issues can be overcome or at least mitigated by using smart charging, which is capable of charging vehicles in a way that does not negatively impact the grid [13]. Smart charging prevents the smart parking facility's maximum energy capacity from being exceeded by dynamically managing the EVs connected simultaneously. At the same time, it enables the integration of renewable energy sources by promoting local self-consumption [14].

It is therefore a form of energy sharing, allowing charging operators to proportionally distribute the smart parking facility's energy capacity among all active charging stations in the parking lot. In this way, smart charging enables optimal energy distribution, which also benefits the power grid and the environment.

If the ability to feed energy back into the grid is added to unidirectional smart charging—known as V1G—then it is called bidirectional charging, identified as V2G [15]. In fact, V2G currently allows EVs to charge during off-peak hours and feed energy back into the grid during peak hours when there is a demand for additional power. This charging method is ideal for smart parking lots, as cars remain parked 95% of the day; therefore, with careful planning and the right infrastructure, parked and connected EVs could become massive power banks, helping to stabilize the grid when necessary.

RECs represent a further step toward sustainable and distributed energy management. They were recently regulated in Italy through the CAREC decree [16], which implements the requirements of the European RED II Directive and promotes the spread of collective self-consumption and the emergence of RECs at the local level. RECs, defined as local groups of consumers and producers connected to the same HV/MV substation who share the energy produced by one or more renewable energy plants, are established with the goal of optimizing collective self-consumption, reducing dependence on fossil fuels, lowering energy costs, and increasing the resilience of local grids. However, if not properly designed, they risk failing to achieve their intended objectives [17].

In this context, the integration of smart parking facilities equipped with smart charging stations for EVs represents a strategic opportunity. In fact, current regulations explicitly allow for the inclusion of energy storage systems and EVs among the infrastructure that can participate in self-consumption and energy sharing within RECs, provided they are located within the boundaries of the relevant primary substation. The bidirectional exchange of energy between vehicles or Energy Storage Systems (ESS) and the local grid can therefore transform the parking lot into an active player in the community, capable of absorbing excess energy produced by renewable energy systems during daylight hours and returning it to the grid or to other community members during times of peak demand.

In the following, with the aim of achieving a more efficient use of the infrastructure and energy resources within the RECs, a method for sizing the photovoltaic system and ESS to be installed within V2G smart parking facilities serving the RECs is presented. Next, an optimization model is developed and experimentally validated for the operational management of EVs as a flexibility resource for participation in local flexibility markets.

3.4.2 Optimal sizing of the REC's energy resources

Studying the impact of RECs on the distribution system is crucial for understanding the changes they introduce in the technical management of the power grid [18]. RECs promote the local production and consumption of renewable energy, primarily photovoltaic, by integrating into the low- and medium-voltage levels of the grid. From a technical standpoint, the introduction of uncontrolled distributed generation can lead to significant variations in power flows, which may become bidirectional, causing local overvoltages, line congestion, frequency fluctuations, and difficulties in coordinating protections.

Referring to the simplified REC model shown in Figure 3.4, the aim of the proposed method is to select the size of the photovoltaic system and ESS to be included within a smart parking facility serving a REC in order to maximize local self-consumption and thereby reduce the impact on the grid.

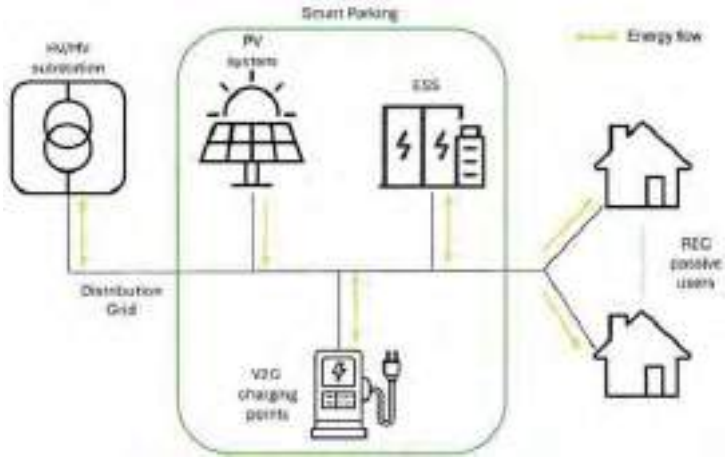

Figure 3.4 REC Architecture Under Study

Maximizing local self-consumption within an REC means using internally generated renewable energy as much as possible, in real time. This helps reduce costs associated with grid usage, increases incentives related to energy sharing, and, through the use of an ESS, prevents the sale of unused energy at a low price. Consequently, economic optimization within a REC directly results in maximizing local self-consumption and thereby reducing the impact on the distribution grid.

Given the Italian regulatory framework, for the REC model shown in Figure 4, the total annual cost can be defined as:

$$C_0 = c^{ess} \cdot Q + c^{pv} \cdot P + \sum_{h=1}^{3600} \left(P_h^{buy} \cdot q_h^{g2l} - P_h^{sell} \cdot q_t^{l2g} - P_h^{inc} \cdot q_h^{sh} \right) \quad (1)$$

Where:

- c^{ess} and c^{pv} are the annualized investment costs for the battery [€/kWh] and the photovoltaic system [€/kW], respectively, calculated by multiplying the average unit cost by the sum of the depreciation, maintenance, and inflation factors;
- Q is the capacity of the ESS [kWh];
- P is the PV size [kW];
- P_h^{buy}, P_h^{sell}, e P_h^{inc} [€/kWh] are respectively, the purchase price, the sale price, and the price associated with the energy-sharing incentive at time *h;*
- q_h^{g2l} is the energy consumed by the REC from the grid at time *h* [kWh], calculated as the difference between the REC's demand, its generation, and the energy provided by the ESS;
- q_h^{l2g} is the energy injected into the grid by the REC at time *h* [kWh], calculated as the difference between generation, energy stored in the ESS, and the REC's demand;
- q_h^{sh} indicates the net energy flow [kWh], defined as the minimum value at the reference hour *h* between the REC's total consumption and total generation.

The following constraint on the installed capacity of the photovoltaic system is defined:

$$P_{pv,\,max} = \frac{E_{rec}}{h_{eq} \cdot K} \quad (2)$$

Where:

- $P_{pv,max}$ is the maximum photovoltaic power that can be installed (kW);
- E_{rec} is the total average daily REC consumption (kWh);
- h_{eq} represents the equivalent hours of daily photovoltaic production for the month considered;
- K is the overall efficiency of the photovoltaic system, conventionally assumed to be 0.75.

To minimize ESS wear, the state of charge (SOC) should be maintained between 20% and 90% at all times, and only one charge/discharge cycle should be performed per day; therefore:

$$SOC_d \geq SOC_{d'} \tag{3}$$

Where:

- SOC_d is the ESS capacity at the start of the day;
- $SOC_{d'}$ is the ESS capacity at the end of the day.

Finally, the size of the photovoltaic system and ESS to be installed in a smart parking facility serving the REC is calculated by identifying the optimal combination of photovoltaic capacity and ESS size that minimizes the REC's costs:

$$OF = min\ C_0 \tag{4}$$

In this way, it is therefore possible:

1. maximize the sharing of energy produced within the REC, so as to supply the users in the smart parking and the buildings that are part of the REC;
2. minimize the electricity consumption from the grid;
3. optimize ESS management to be able to ensure coverage of the REC's loads during nighttime hours when PV is not producing;
4. to reduce CO_2 emissions, which is the main goal of RECs.

Given the REC's consumption, the ESS capacity that can be charged up to SOC_{max} is calculated for each value of the installable PV power.
The procedure can result in the identification of several capacity values that satisfy the desired condition; from these, the maximum value is chosen, i.e., the one that allows the largest amount of energy to be stored.
This choice, even if it involves a higher initial investment, allows maximizing the energy sharing and thus consuming less energy from the grid.
With a consequent increase in the incentive and a reduction of the total annual cost.

Finally, to assess the economic feasibility of the installation, the difference between the annual costs of the REC in the absence C' and in the presence of PV and ESS C_0 is calculated:

$$\Delta C = C' - C_0 \tag{5}$$

A negative value of *DC* or otherwise a very low value is identifying the affordability of the investment.

3.4.3 Case Study: University of Palermo Campus

The main objective is to reduce the overall REC's costs. According to the proposed method, this means maximizing energy sharing while minimizing the amount of energy consumed from the grid to meet the REC's energy needs, through the optimal selection of the photovoltaic system's size and the ESS's capacity. To evaluate its effectiveness, the presented method was implemented in a MATLAB environment and applied to size the PV system and ESS to be installed in the smart parking facility to be integrated into a REC on the campus of the University of Palermo (UNIPA).

Figure 3.5. Smart Parking UNIPA

The university campus's electrical grid consists of a 20-kV cable line. The line originates from the HV/MV substation named “Cappuccini” and supplies power to 11 secondary substations located within the campus. The MV/LV substation named “Carrubba University” is designated to supply electricity to Building 9 and the adjacent area, including the School of Architecture. This area is the focus of the study aimed at implementing a REC consisting of:

- A smart parking lot, part of which is dedicated to charging EVs;
- The complex of buildings adjacent to the parking lot;
- A PV system;
- An ESS.

To test the effectiveness of the proposed method, two scenarios are analyzed:

- **Scenario 1**: EVs are considered loads; V1G configuration;
- **Scenario 2**: EVs batteries can be used to provide ancillary services to the grid and partially power evening loads; V2G configuration.

Scenario 1: V1G

The starting data for optimally sizing the photovoltaic system and ESS to be installed in the smart parking lot are the power consumption of the loads within the REC, including vehicles owned by staff and students that are parked there, and the specific power output of the photovoltaic system.

The total load diagram for the buildings adjacent to the smart parking lot and the vehicles shows a difference between weekdays and weekends. From Monday to Friday, power demand is initially stable between 25 and 30 kW until 7:00 a.m., then rises to a peak of approximately 70 kW between 10:00 a.m. and 12:00 p.m. It subsequently decreases gradually, falling below 40 kW around 7:00 p.m., coinciding with the campus closing. On weekends, however, the trend remains stable between 25 and 30 kW, with lower values due to the reduced number of people in the REC buildings.

The specific power output of the photovoltaic system to be installed can be estimated for various months of the year using the online PVGis tool.

These data were entered into the model, and the results are shown in Figure 3.6.

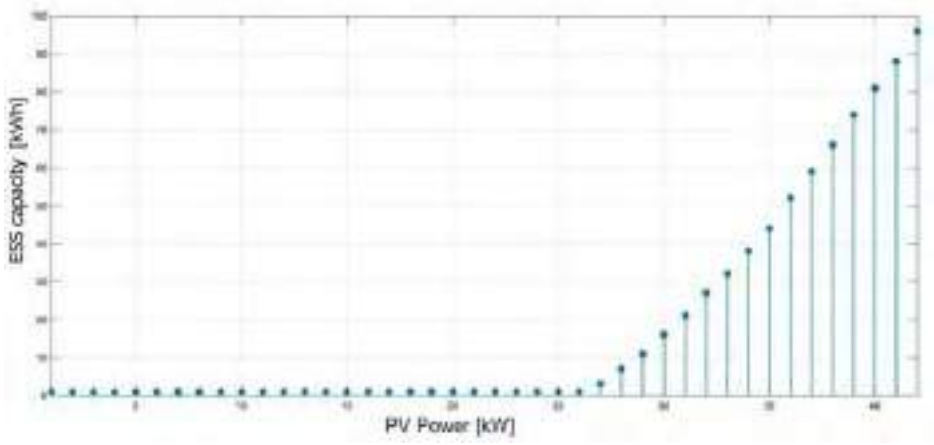

Figure 3.6 Optimal ESS capacity depending on the PV power installed

Specifically, Figure 3.6 shows that as the installed photovoltaic capacity varies, the algorithm selects the ESS capacity to minimize both the injection of renewable energy into the grid and the consumption of grid power by REC users. The ESS capacity value is 1 kWh up to an installed PV capacity of 27 kW, then begins to increase as the size of the PV system increases. The maximum value reached at 42 kW is 97 kWh. Higher values would result in excessively high costs.

The following figures show the energy flows during a typical weekday (Figure 3.7) and weekend (Figure 3.8) in June 2024 for the analyzed REC following the installation of the PV system and ESS, calculated by considering vehicle charging during production hours to maximize energy sharing.

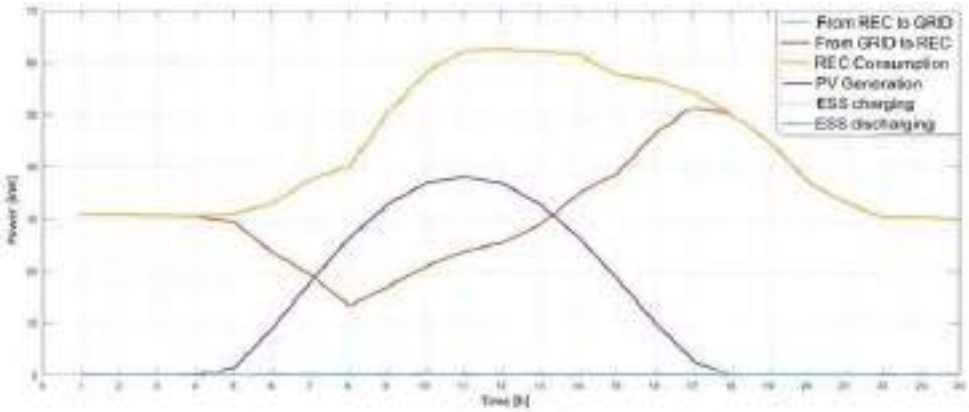

Figure 3.7 REC Energy Flows on Weekdays in June 2024

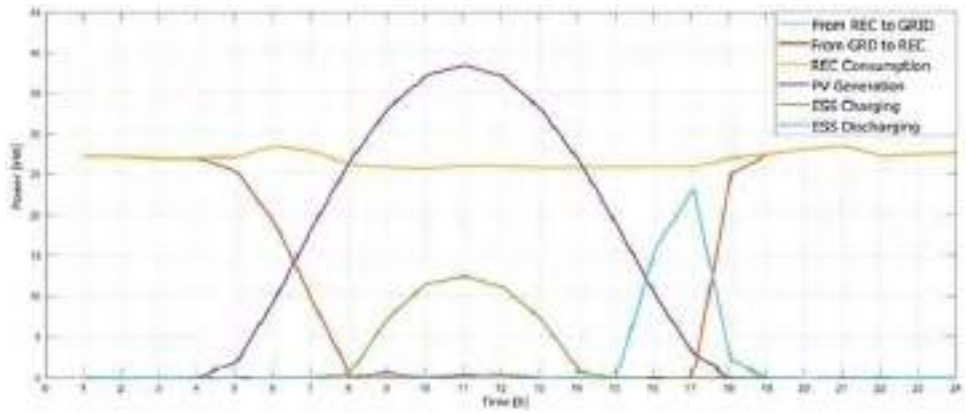

Figure 3.8 REC Energy Flows on Weekend in June 2024

Figure 3.7 shows that during the week, since demand consistently exceeds generation, all the energy produced is consumed by the REC, minimizing consumption from the grid, and the ESS is never charged. Meanwhile, Figure 3.8 shows that, during weekends, due to the reduced load, part of the energy produced is used to charge the ESS, and to reduce consumption from the grid, the stored energy is then used to power the REC.
The following Table 3.2 shows all the energy and economic quantities evaluated by the algorithm:

Table 3.2: REC UNIPA – Summary of Energy and Economic Quantities

Category	Description	Value
PV and ESS Size		
	PV Power [kW]	42.00
	ESS Capacity [kWh]	97.00
Energy Quantities		
	PV Generation [kWh/year]	86,715.00
	PV Energy Consumption [kWh/year]	86,715.00
	Energy Sold [kWh/year]	0
	Energy Sharing [kWh/year]	89,992.00
	Energy Consumed from Grid [kWh/year]	302,930.00
Economic Quantities		
	Self-consumption Savings [€/year]	24,117.00
	REC Incentive [€/year]	9,899.10
	ARERA Incentive [€/year]	7,199.30
	Energy Sales [€/year]	0
	Energy Purchases [€/year]	59,159.00
	Benefits [€/year]	41,216.00
	System Investment Cost [€/year]	85,207.00
Other Quantities		
	Payback Time [years]	5 years and 1 months
	PI (Profitability Index)	15.32
	CO_2 Avoided in 20 Years [Tons]	479.19

The results show that optimizing the sizing of the photovoltaic system and ESS—based on an analysis of REC users' energy consumption and by scheduling vehicle charging during peak production hours—can reduce overall costs. Specifically, for the case study, an investment of nearly €85,000 yields annual energy purchase savings of approximately €25,000, a payback period of 5 years and 1 month, and a CO_2 reduction of about 480 tons over 20 years.
The analysis of the first V1G scenario reveals several technical aspects worthy of further investigation that are directly linked to the opportunity for V2G integration:

- **Economic Sensitivity Analysis**: Changes in the energy purchase price (±10%) affect the payback period but do not drastically alter the optimal sizing solution. However, rising energy prices make investing in additional storage capacity more attractive, paving the way for V2G integration as a cost-effective alternative.
- **Seasonal Management of the ESS**: During the winter months, with fewer equivalent hours of photovoltaic generation (heq), the ESS is underutilized. This highlights potential for improvement through additional and more flexible storage resources, such as V2G vehicle batteries, which could offset seasonal variability.
- **Impact on Grid Quality:** Despite the absence of power fed into the grid (Energy Sold = 0), the future increase in photovoltaic capacity will require careful assessment of local voltage profiles and protection coordination. V2G integration can make a positive contribution to local voltage regulation through the coordinated management of reactive power flows.
- **Unused Flexibility Potential:** Analysis of energy flows reveals time windows in which the REC could offer flexibility services to the power system. On weekends, when demand is lower than generation, there is scope to modulate loads according to grid requirements. This observation serves as the conceptual bridge to V2G Scenario 2.

Scenario 2: V2G Integration

At this point, it is explored what happens when EVs connected to charging stations are included, with the ability to exchange energy with the grid in both directions.
The integration of V2G technology requires extending the model to include:

Additional variables for EVs:

- $SOC_v(t)$: Vehicle *v* charge state at time *t;*
- $P_{v,ch}(t)$, $P_{v,dis}(t)$: vehicle charging and discharging power;
- $x_v(t) \in \{0,1\}$: binary variable for vehicle availability.

V2G operational constraints:

- $SOC_{v,\,min} \leq SOC_v(t) \leq SOC_{v,max}$
- $SOC_v(t_{dep}) \geq SOC_{req,v}$ *(Minimum SOC at startup)*
- $0 \leq P_{v,ch}(t) \leq x_v(t) \times P_{v,max}$
- $0 \leq P_{v,dis}(t) \leq y_v(t) \times P_{v,max}$

Additional costs:

- Battery degradation cost: $c_{deg} \times E_{v2g}(t)$
- Owners' remuneration: $r_v(t)$

The extended economic model becomes:

$$C_{ext} = C_0 + \sum_v \sum_t (c_{deg} \cdot e_v^{v2g}(t) - r_v(t)) \tag{6}$$

Considering the presence of 5 vehicles, each with a battery capacity of 30 kWh and a maximum charging and discharging power of 5 kW, and assuming that each makes 30% of its capacity available, 45 kWh of energy would be available. This energy could be used both during the day to address fluctuations in power generation and in the late afternoon/evening to partially supply the REC's loads.
The integration of V2G technology would result in a significant reduction in the required ESS capacity, as part of the energy would be dynamically supplied by the connected EVs. Specifically, the availability of an additional 45 kWh supplied by the EVs would allow the stationary battery to be downsized from 97 kWh to approximately 52 kWh, while maintaining the flexibility necessary for managing supply and demand within the REC.
This reduction results in a significant decrease in investment costs, estimated at approximately €60,000 compared to the initial €85,000. In addition to the direct economic benefit, there is also an improvement in the profitability ratio and a reduction in the payback period, which would be shortened to approximately 3 years and 5 months.
From an operational perspective, using vehicles as a flexible energy resource also improves the system's resilience and can help optimize self-consumption and encourage active user participation in community management. However, this solution introduces new organizational and technical complexities, such as variability in vehicle availability, the need to establish financial compensation mechanisms for owners, and the implementation of advanced control systems to coordinate energy injection and withdrawal.
To mitigate these critical issues, a viable strategy could be the use of university service vehicles, dedicated in part or entirely to the community's needs. Such vehicles, having more predictable and controllable usage patterns, could provide a stable resource for load shifting operations, contributing structurally to the community's energy balance.

Comparative Analysis of the Two Scenarios
A comparison of the two scenarios clearly highlights the advantages of V2G integration:
Economic Aspects:

- Reduction in initial investment: 30% (from €85,000 to ~€55,000)
- Improved payback period: from 5 years and 1 month to 3 years and 5 months
- Increased profitability index due to lower capital tied up

Technical Aspects:

- Maintenance of energy performance (self-consumption, sharing)
- Greater operational flexibility through distributed storage management
- Potential participation in local flexibility markets

Environmental Aspects:

- Maintenance of CO_2 reduction benefits
- Optimization of existing resource utilization (vehicle batteries)
- Reduction in the need for stationary storage

3.4.4 V2G Management for Flexibility Markets

Italy has recently opened up the opportunity for end users to participate in the Local Flexibility Market (LFM). The LFM is a tool introduced to enable smarter and more dynamic management of the electricity system, especially at the local level [19]. The basic idea is simple: when congestion or an imbalance between energy production and consumption occurs in a given area, users connected to the grid who are able to provide flexibility can be asked to temporarily adjust their consumption or generation behavior in exchange for compensation. The LFM was launched in 2021 following a decision by the Italian regulator (ARERA, Resolution 352/2021/R/eel), which assigns local distributors the task of identifying areas with flexibility needs and collecting offers from entities willing to provide it, thereby introducing new players such as flexibility providers and aggregators. Resolution 372/2023/R/eel approved an Areti pilot project, and, pursuant to dedicated regulations, the Energy Markets Operator (GME) was designated as the operator of the trading platform. Finally, Resolution 420/2023/R/eel established the financial terms for participation and for the remuneration of the services offered.
This mechanism is designed to actively involve even small-scale producers and consumers, particularly those located near distributed generation facilities, such as prosumers with solar panels, users who install home batteries, heat pumps, or EV charging systems. In this scenario, RECs, whose structure and mission are particularly well-suited to providing flexibility services, play a central role. Participation in the LFM would allow RECs to:

- receive compensation for their willingness to reduce or shift consumption or generation at specific times;
- contribute to the stability of the local power system;
- increase the economic return for their members;
- strengthen their role in the energy transition.

However, the current ability of a REC to provide flexibility is still limited. In most cases, RECs rely on small-scale photovoltaic systems (often without storage) and on residential loads that are difficult to predict or manage. Flexible loads such as heat pumps, smart appliances, or controlled charging systems for EVs are not yet widely adopted and are difficult to coordinate efficiently. If RECs are to evolve from simple energy-sharing platforms into active players in the flexibility market, it is therefore necessary to introduce technologies capable of providing a concrete, measurable, and timely contribution.
In this context, the integration of EVs into RECs is recognized as one of the most effective solutions for increasing flexibility, self-consumption, and grid resilience [20]. In particular, V2G systems allow vehicles to function as distributed storage units, modulating in real time the power absorbed (charging) or fed into the grid (discharging), and thus providing services such as frequency regulation, demand peak reduction, and congestion mitigation [21], [22]. This makes it possible not only to utilize excess photovoltaic energy during charging but also to manage the grid interaction profile more flexibly, contributing to local balancing [23].
Several studies have shown that smart charging and V2G can:

1. increase local self-consumption of solar power;
2. reduce overloads on distribution grids;
3. promote the decarbonization of transportation [23], [24].

In [25], for example, vehicles are coordinated by an aggregator that maximizes collective economic benefit by simultaneously participating in energy and ancillary service markets. Other studies focus on scheduling algorithms that account for user mobility constraints (arrival and departure times, minimum required charge level) and respond to price signals or grid congestion signals [26], [27].

In parallel, several pilot projects have validated the technical feasibility of V2G in the field. The Danish Parker project demonstrated the suitability of vehicle fleets for frequency regulation [28], while initiatives such as Electric Nation in the United Kingdom analyzed the impact of smart charging on the low-voltage grid [29]. Other European projects have explored the integration of EVs and renewable energy generation in neighborhood or apartment complex settings, highlighting the potential of energy communities to coordinate these resources [30].

In terms of flexibility, EVs in a V2G configuration act as programmable resources, capable of rapidly adjusting the power they draw or supply while adhering to constraints related to SoC and the owner's mobility needs. In a REC context, the deployment of V2G EVs transforms charging points into active energy nodes, capable of interacting with local renewable generation and with price or grid congestion signals.
Despite these advances, the literature explicitly addressing REC participation in local flexibility markets, by jointly considering vehicle availability and SoC constraints, shared energy maximization objectives, and specific LFM rules, remains limited.
For this reason, we propose an optimization model for RECs with V2G EVs, capable of simultaneously maximizing internal energy sharing and the ability to offer flexibility as an aggregate. The model coordinates prosumers and consumers equipped with V2G EVs, with the aim of increasing the community's shared energy while simultaneously ensuring a power margin for participation in the LFM. The methodology was tested at the SMGLab of the University of Palermo, emulating a portion of the community in the laboratory.

Optimization Model for V2G Flexibility
The primary objective of a REC is to consume (virtually), hour by hour, all the energy produced by the systems within the configuration.
Outside of photovoltaic production hours, the REC equipped with EVs connected via V2G can primarily provide downward flexibility (from the grid's perspective), increasing its own consumption through vehicle charging or reducing the energy fed back into the grid.
During production hours, the community can offer:

- downward flexibility (reduction in net load or increase in feed-in) if production exceeds consumption;
- upward flexibility (increase in net load) if consumption exceeds production.

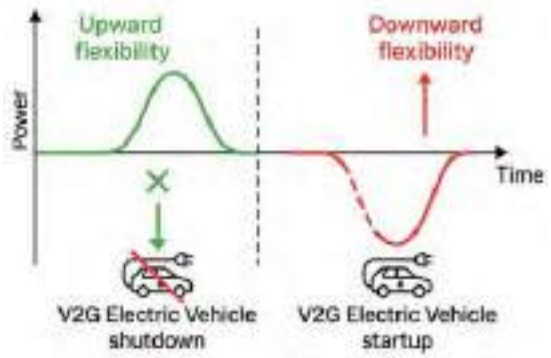

Figure 3.9: flexibility provided by V2G EVs

The proposed model aims to simultaneously maximize, over the next 24 hours, based on forecasts of solar power generation and user consumption:

1. the amount of energy shared within the community;
2. the aggregate flexibility that the community can offer to the market, defined as the potential variation (upward or downward) in electricity demand relative to the optimal profile.

To this end, a multi-objective formulation based on the weighted sum method is adopted, which linearly combines the hourly sum of shared energy with the sum of aggregate flexibility.

The problem can be formulated using a rolling horizon, so that decisions are periodically updated as forecasts improve.
Consider a REC composed of prosumers equipped with photovoltaic systems, passive consumers without generation or flexible capacity, and flexible users equipped with V2G EVs.
For simplicity, the model focuses here on the power capacity and hourly availability of connected vehicles, assuming that SoC and mobility constraints have already been translated into time windows for use and maximum allowed power levels.

Let's define:

- $T = \{0, 1, \ldots, 23\}$: total optimization hours;
- H: users with V2G-enabled electric vehicles;
- G(t): REC's aggregated PV generation profile at time *t*;
- $C_i(t)$: user *i* consumption profile at time *t*;
- $C_{tot}(t) = \Sigma_{i \in \{1,\ldots,N\}} Ci(t)$: total demand from all users at time *t*, excluding exchanges with vehicles;
- P_h^{ch}: maximum charging power of the user's vehicle *h* [kW];
- P_h^{dis}: maximum power fed back to the user's vehicle's power grid [kW];
- $x_{h,t}^{ch} \in \{0,1\}$: binary variable indicating whether vehicle *h* is charging at time *t*;
- $x_{h,t}^{dis} \in \{0,1\}$: binary variable indicating whether vehicle *h* is discharging (V2G) at time *t*;
- $P_h(t)$: net power exchanged between vehicle *h* and the grid at time *t* (positive during charging, negative during discharging);
- $E_{sharing}(t)$: shared renewable energy at time *t*;
- $F^+(t)$, $F^-(t)$: upward and downward flexibility at time *t*.

To prevent a vehicle from being both charging and discharging at the same time, the following is required:

$$x_{h,t}^{\mathrm{ch}} + x_{h,t}^{\mathrm{dis}} \leq 1 \quad \forall h \in H,\ t \in T. \tag{7}$$

The power exchanged by vehicle *h* is limited by:

$$0 \leq P_h(t) \leq x_{h,t}^{\mathrm{ch}}\, P_h^{\mathrm{ch}}, \tag{8}$$

$$-x_{h,t}^{\mathrm{dis}}\, P_h^{\mathrm{dis}} \leq P_h(t) \leq P_h^{\mathrm{ch}}, \tag{9}$$

In order to calculate shared energy, the REC's energy balance takes into account PV generation and user consumption, including consumption related to vehicle charging.
The conditions for sharing are:

$$E_{\mathrm{sharing}}(t) \leq G(t), \quad \forall t \in T. \tag{10}$$

$$E_{\mathrm{sharing}}(t) \leq C_{\mathrm{tot}}(t) + \sum_{h \in H} \max\{P_h(t), 0\}, \quad \forall t \in T \tag{11}$$

In MILP form, the term $\max\{P_h(t), 0\}$ can be represented linearly by introducing appropriate auxiliary variables; in this formulation, the key concept is that the charging power of vehicles supplied by photovoltaics contributes to the increase in shared energy.
With regard to flexibility, a distinction is made between situations of surplus and deficit in renewable generation.
If $G(t) \geq C_{tot}(t)$ (generation surplus), the community can primarily provide upward flexibility $F^+(t)$ by reducing vehicle charging or activating V2G discharge:

$$F^+(t) \leq G(t) - C_{\mathrm{tot}}(t), \tag{12}$$

$$F^{+}(t) \leq \sum_{h \in H} \left[x_{h,t}^{ch} P_h^{ch} + x_{h,t}^{dis} P_h^{dis} \right] \tag{13}$$

$$F^{-}(t) = 0. \tag{14}$$

If, on the other hand, G(t) < C_{tot}(t) (generation deficit), downward flexibility F^{-}(t) is mainly available, achieved by increasing charging or reducing the power delivered via V2G:

$$F^{-}(t) \leq \sum_{h \in H} \left[P_h^{ch} - \max\{P_h(t), 0\} \right], \tag{15}$$

$$F^{+}(t) = 0. \tag{16}$$

The binary decision variables are therefore:

$$x_{h,t}^{ch}, x_{h,t}^{dis} \in \{0,1\}, \quad \forall h \in H, \; t \in T. \tag{17}$$

The optimization problem, which includes both continuous variables (power, energy) and binary variables (vehicle charge/discharge status), is formulated as a Multi-Objective Mixed-Integer Linear Programming (MO-MILP) problem, solved using a weighted sum approach.
The multi-objective function is defined as:

$$OF = \max \left\{ \alpha \sum_{t \in T} E_{sharing}(t) + (1-\alpha) \sum_{t \in T} \left[F^{+}(t) + F^{-}(t) \right] \right\} \tag{18}$$

Where α ∈ [0,1] is a weighting parameter that determines the balance between the two objectives.
The REC optimization problem involves a trade-off between maximizing the shared energy and the flexibility offered by the REC.
By varying α, it is possible to explore different solutions, in which the relative importance of the two objectives reflects the community's priorities, for example based on the incentive framework or local grid conditions.
The choice of the weighted sum approach is motivated by its simplicity of implementation and the transparency in interpreting the results.
The result of the optimization is a 24-element hourly vector that describes, for each electric vehicle:

- the charging/discharging states (V2G) at various times of the day;
- the energy shared by the community;
- the hourly flexibility that the REC can make available to the LFM.

3.4.5 Case Study and Results

To evaluate the performance of the methodology described in the previous section in a context representative of a small urban community or a medium-sized town, a REC comprising 50 users was analyzed.
The first step involved selecting the types of users and the capacities of the renewable energy systems.
Only residential users with consumption patterns similar to those used by the Energy Services Operator (GSE) to estimate hourly electricity consumption curves for the year 2025 were considered [31].
For the size of the photovoltaic systems, reference was made to the criteria proposed in [17], selecting a total capacity optimized based on the number of users.
Thus, a REC was configured with 50 residential users and 67.5 kWp of total photovoltaic capacity.

Generation potential was estimated using the online tool PVGIS [32].
The community is composed of the following:

- 15 prosumers with 4.5 kWp PV systems;
- 20 passive users;
- 15 users with V2G electric vehicles, each with a connection capacity of 4 kW.

The REC was replicated at the SMGLab at the University of Palermo. Forty-eight users were simulated using software models, while a prosumer and a flexible user with an electric vehicle were physically emulated using the test bench installed within the laboratory. The test bench was designed to emulate a "smart" prosumer capable of optimally managing production and consumption for participation in ancillary services or energy sharing within a REC.
It allows for the simulation of both single-phase and three-phase loads and, if necessary, up to three users connected to the same node of a low-voltage network.
The setup, located within the SMGLab, includes:

- an electrical panel with protection, isolation, and measurement devices;
- an isolation transformer, used to enhance operator safety;
- six variable resistance banks, for simulating passive loads of varying magnitudes;
- a speed-controlled single-phase asynchronous motor, for simulating active loads;
- a photovoltaic inverter connected to a DC generator, capable of replicating the behavior of a PV array and a lithium-ion battery storage system;
- a microcontroller-based control system (Raspberry Pi 4) for exchanging data and commands with the various devices.

By coordinating the control of the inverter, the DC generator, and the resistive loads, it is possible to emulate a user that flexibly generates and consumes energy according to the profiles established by the optimization algorithm.
EV charging and V2G mode were emulated using the bidirectional inverter and the storage system, imposing power limits consistent with a 4 kW home charging point. The prosumer, on the other hand, was simulated using the PV inverter and three of the six resistor banks, while the flexible user with an EV utilized the other three resistor banks combined with the storage system, representing the vehicle's battery.
The optimization algorithm was implemented in Python and run on the test bench control system.
The PuLP library was used to solve the MILP problem; it provides a declarative interface for defining decision variables, the objective function, and constraints, and allows integration with various external solvers.
In this work, the Coin-or Branch and Cut (CBC) solver was used, selected for its ability to effectively handle problems with binary variables and for its native integration with PuLP.
Taking a typical day in July 2025 as a reference, Figure 3.10 shows the total REC production capacity (sum of prosumers' PV output), the energy fed into the grid, total user consumption (excluding contributions from vehicles), and the shared energy in the absence of optimization.

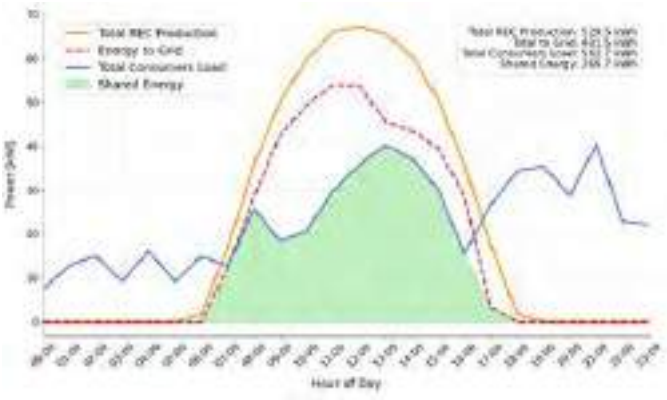

Figure 3.10: REC energy flows before optimization.

The execution of the optimization algorithm provides the strategy for using EVs during periods of photovoltaic power generation, taking into account the weight α assigned to energy sharing relative to flexibility.
Figure 3.11Figure 3.12 and Figure 3.13 show the results in terms of shared energy and aggregate flexibility for three different values of α.

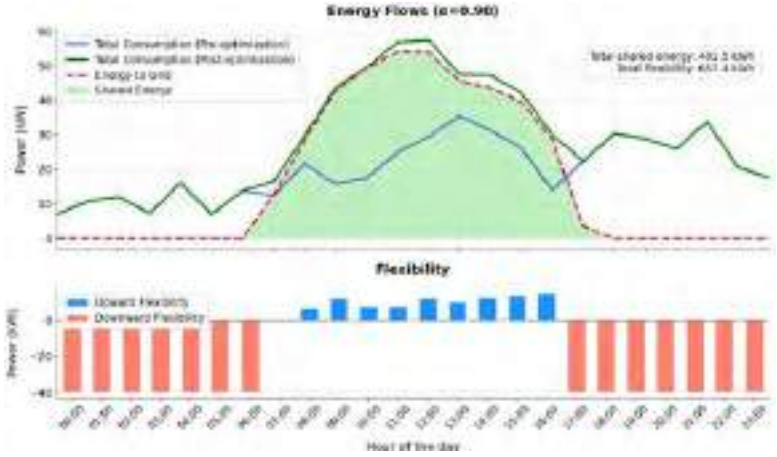

Figure 3.11: Optimization results with α=0.9

Figure 3.12: Optimization results with α=0.5

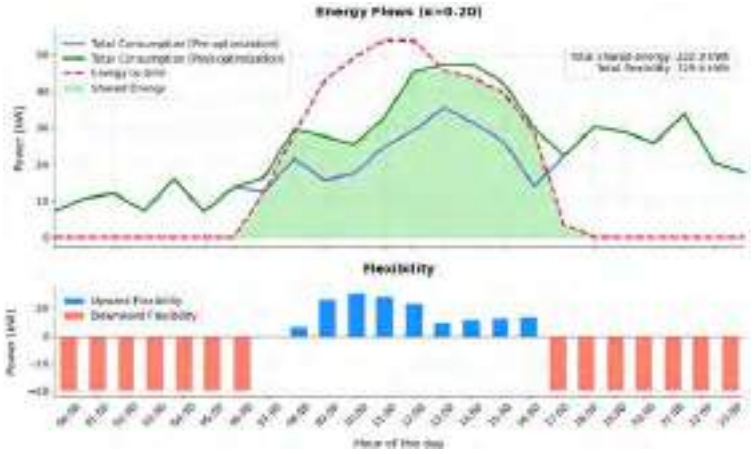

Figure 3.13: Optimization results with α=0.2

The figures show how the shared energy and the amount of available flexibility vary as the weight assigned to the objectives changes.
Outside of peak production hours, vehicles are generally kept in a state of inactivity with respect to the grid, preserving the battery while ensuring a potential margin of flexibility. During the middle of the day, when PV production is highest, the optimization determines for each vehicle whether it is better to prioritize charging (increasing shared energy) or to maintain a power reserve for participation in the LFM.
In the case where $\alpha = 0.5$, the model provides a balanced compromise between maximizing shared energy and flexibility.

For the flexible user emulated in the laboratory, the results indicate specific time windows for charging and, during certain intervals, the possibility of providing V2G services without compromising the charge level required for vehicle use.
Figure 3.15 compares the user's load profile (including EV charging) before and after applying the optimization algorithm.

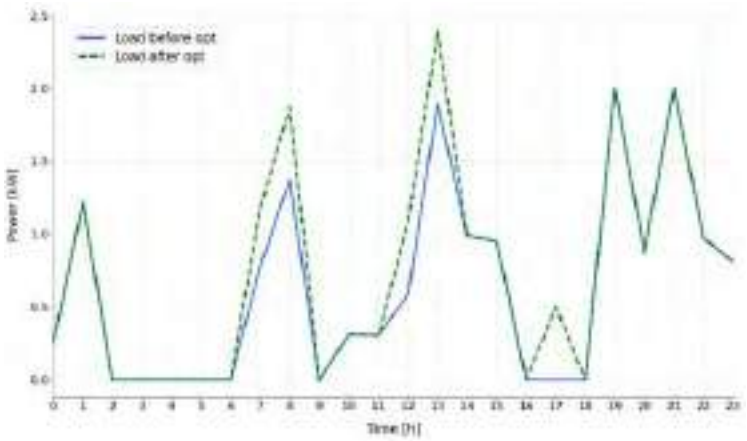

Figure 3.14: User load profile emulated in the SMGLab

It can be seen that, following the optimization, vehicle charging is concentrated primarily during hours of high PV production, reducing evening power withdrawals and increasing the amount of energy actually shared within the REC. At the same time, a margin of available power is maintained during certain time slots, which can be used to adjust the power exchange profile with the grid at the LFM's request.

3.4.6 Conclusions

The two studies confirm the strategic role that distributed generation, energy storage, and electric mobility technologies can play within RECs. In the first study, the integration of smart parking systems equipped with photovoltaic arrays and stationary storage systems demonstrated how an optimized sizing and management approach can significantly increase local self-consumption, reduce grid draw, and simultaneously improve economic and environmental performance. The case study of the University of Palermo campus highlighted particularly favorable economic indicators, with short payback periods and a significant reduction in energy costs and CO_2 emissions, further improved by the introduction of V2G technology, which reduces the required stationary storage capacity and accelerates the payback period.
The second study explored the potential of EVs in V2G configurations as a flexibility resource within RECs, with particular reference toLFM. Using a multi-objective optimization model, validated through experimental tests at the SMGLab of the University of Palermo, it was demonstrated that coordinated management of EV charging and discharging allows for increased energy sharing and makes a significant contribution to grid flexibility. The weight parameter α emerges as a key element for balancing the maximization of energy sharing with the remuneration of

flexibility services, highlighting how technical aspects are closely intertwined with economic and regulatory ones. Taken together, the results of the two studies show that the evolution of RECs toward configurations that integrate smart parking, storage systems, and V2G EVs makes it possible to transform the community from a simple group of self-consumers into an active node in the grid, capable of providing ancillary services, leveraging local renewable surpluses, and generating additional economic benefits for its members.
However, significant challenges remain to be addressed in order to make these solutions scalable: upgrading metering and communication infrastructure for real-time control of energy flows, establishing stable and transparent compensation schemes for flexibility services, deploying compatible V2G vehicles and infrastructure, as well as developing contractual tools and advanced control algorithms that ensure both the community's profitability and the fulfillment of users' mobility needs.
Future developments may involve the integration of additional flexible resources, the improvement of production and consumption forecasting models, the testing of models based on vehicle fleets with predictable usage profiles, and the extension of analysis to multi-community scenarios and coordinated participation in various markets (energy, balancing, ancillary services).

3.5 Distributed PV Control and Voltage Management in LV Networks

3.5.1 Introduction

The rapid expansion of photovoltaic (PV) systems constitutes a fundamental component of the global transition toward low-carbon energy systems. Due to their decreasing costs and scalability, PV technologies have experienced substantial deployment worldwide and are expected to dominate future installed generation capacity. However, the increasing penetration of PV generation introduces significant operational challenges for power systems, particularly at the distribution level, where networks were not originally designed for high levels of decentralized generation.
One of the most critical challenges associated with high PV penetration is the occurrence of operational constraints, including voltage rise, reverse power flow, and limited hosting capacity. In low-voltage (LV) distribution networks, excess PV generation during periods of low demand can lead to overvoltage conditions, which in turn trigger inverter-based control mechanisms that reduce active power output or disconnect generation units entirely [33]. As a consequence, a portion of the available renewable energy is curtailed, resulting in both technical inefficiencies and economic losses for system operators and prosumers.
Curtailment has therefore emerged as a widely adopted operational measure to ensure system security and stability. In modern electricity markets, where energy dispatch is governed by supply–demand dynamics, grid operators may limit PV injection even when generation costs are low, in order to maintain system balance and comply with network constraints [34]. While such actions are necessary to preserve grid reliability, they directly reduce the utilization of renewable resources and negatively impact the financial performance of PV systems through lost revenues and increased levelized costs. To mitigate these challenges, several approaches have been proposed in the literature. Conventional solutions such as network reinforcement or transformer tap-changing are often capital-intensive and lack flexibility in real-time operation. As a result, attention has shifted toward more adaptive strategies based on distributed energy resources. In particular, smart inverter functionalities—such as Volt–Var and Volt–Watt control—enable local voltage regulation by adjusting active and reactive power outputs, thereby reducing the need for excessive curtailment [33]. In parallel, battery energy storage systems offer an additional degree of flexibility by absorbing excess PV generation during peak production periods and releasing it when demand increases, thus alleviating voltage constraints and improving overall energy utilization.
The literature describes a number of applications for the above-mentioned methods. For example, article [35] addresses the issue of voltage surges in low-voltage grids caused by a large number of PV systems in the grid. The voltage at the inverter connection point is measured. If it exceeds the permitted limits, the reactive power is gradually increased. If, despite reaching the maximum reactive power, the correct voltage range is not achieved, a "distress signal" is sent to the other inverters in the same grid. The other inverters operate according to the same algorithm, gradually increasing their share of reactive power until the accepted voltage limits are reached. Only if the cooperation of all inverters in the grid proves ineffective is active power limited to a level that brings the voltage within acceptable limits. The authors [36] take it a step further. The work focuses on optimization aimed at determining a Q(U) curve that maximizes PV active power. The curve is fixed for the

entire following year. PSO was used to determine the curve. The optimization considered the sum of voltage deviations from the nominal value, annual power losses in the grid, and the maximum reactive power of the inverter. In [37], a control strategy similar to that in [35] is implemented, but the authors point out the problem that inverters located farther from the transformer reduce more power, which leads to differences in consumer income. They therefore also proposed a modification of the algorithm, in which they analyzed the sensitivity of voltage to changes in active power (creating a sensitivity matrix) so that energy losses for individual prosumers would be uniform. It turns out, however, that with this algorithm, the total energy reduction in the grid is greater than in the first approach. [38] also addresses the issue of fairness toward prosumers when curtailing PV-generated energy. The authors propose switching the grid on a day-to-day basis so that individual prosumers are sometimes farther from and sometimes closer to the transformer. The paper [39] provides a literature review on methods for limiting PV curtailment; in addition to the solutions mentioned, it also discusses increasing self-consumption through the use of energy storage systems, or without them. Based on the literature review, an infographic was created, as shown in the Figure 3.15.

Figure 3.15.Infographic based on a literature review on PV inverter control strategies for overvoltage conditions.

Despite these advancements, important challenges remain. Local control strategies may lack coordination and lead to suboptimal or unfair curtailment among distributed generators, whereas centralized optimization approaches, although more efficient, require significant communication infrastructure and computational resources. Furthermore, the trade-off between minimizing curtailment and maintaining economic viability has not yet been fully resolved, particularly in realistic distribution network environments with high PV penetration. In this context, the coordinated control of active and reactive power from PV inverters, combined with advanced optimization techniques, represents a promising pathway for enhancing grid performance while maximizing renewable energy utilization. This work focuses on the analysis and optimization of PV inverter operation in radial LV distribution networks, with the objective of minimizing curtailment while ensuring compliance with voltage constraints.

3.5.2 Identification of regulatory potential of PV inverters using laboratory test bench

Laboratory test bench description:
The laboratory test bench of residential microgrid (Figure 3.16) comprises a set of devices that make up a typical microgrid, including a constant-voltage power source, a photovoltaic inverter, a battery energy storage system with a charger, a controllable load, a regenerative power grid simulator, and a connection to the public grid. The entire system is interconnected via the MODBUS TCP/IP protocol for setting and reading parameters, and is metered using a set of power quality analysers and energy meters.

The test setup for tests 1–4 consists of a microgrid in which a DC power supply connected to a photovoltaic inverter serves as the power source, a grid simulator emulates the public grid, and all nodes are equipped with meters.

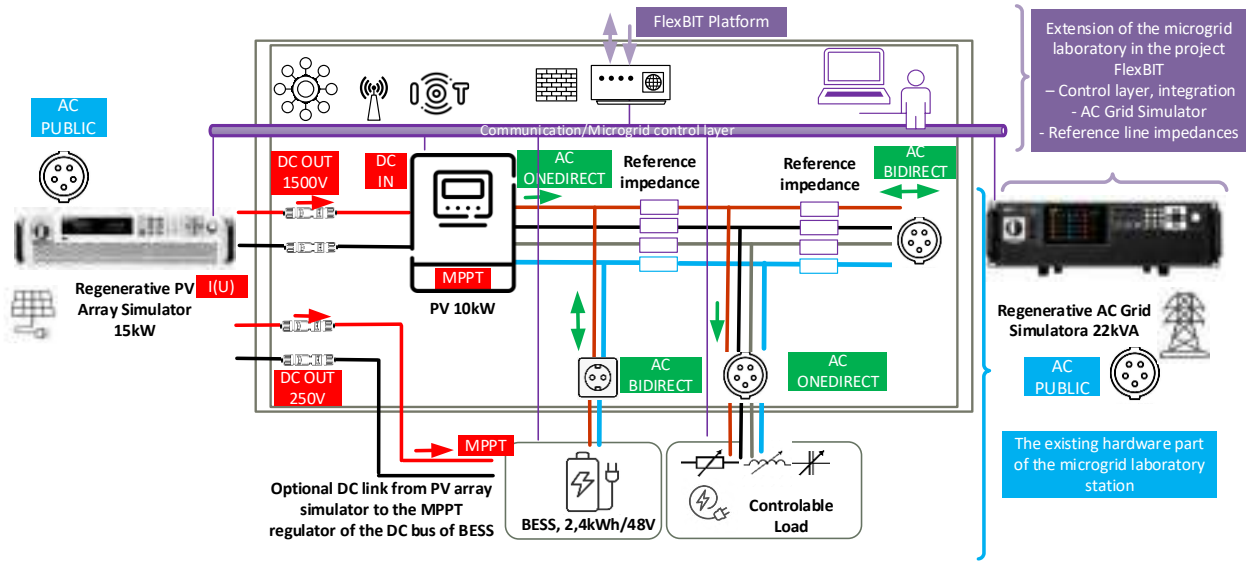

Figure 3.16. General laboratory assets of WUST (Poland) microgrid test bench.

Test 1: Maximum available reactive power

a) b)

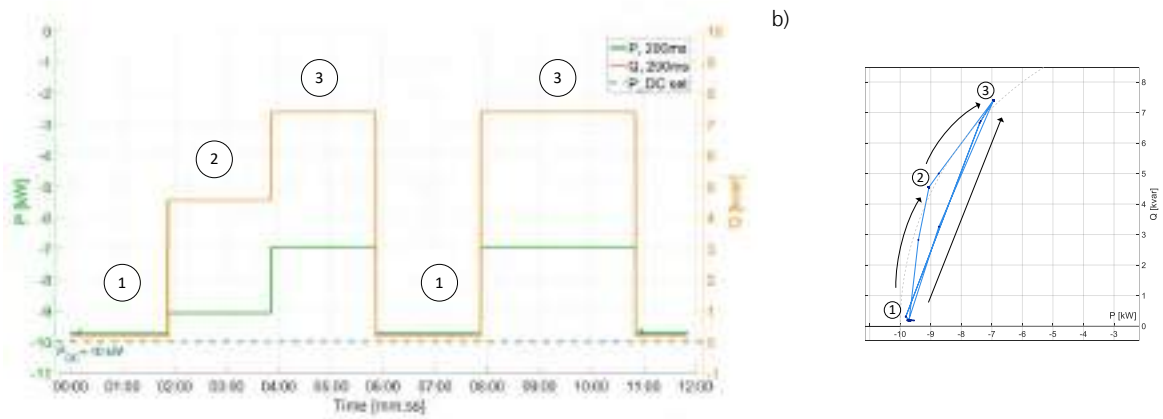

Figure 3.17. Output active and reactive power of PV inverter during reactive power request: a) time response b) PQ plane (1 – no reactive power, 2 – reactive power request expressed by cosfi=0.9, 3 – reactive power request expressed by cosfi=0.7)

.

Test 2: The minimum active power required to maintain the reactive power potential

a) b)

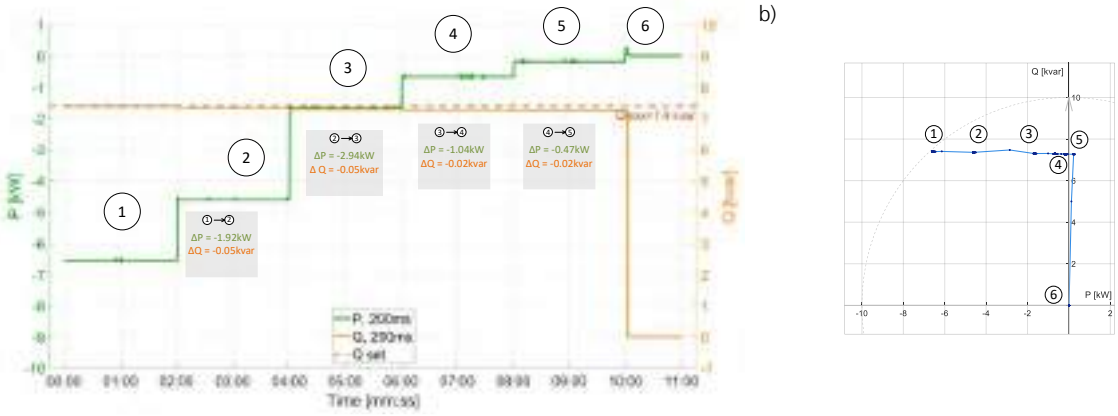

Figure 3.18. Output active and reactive power of PV inverter during a source power reduction: a) time response b) PQ plane (1 – reactive power request expressed by cosfi=0.7, 2 – reactive power request expressed by cosfi=0.5, 3 – reactive power request expressed by cosfi=0.3, 4 - reactive power request expressed by cosfi=0.1, 5 - minimum active power required to sustain the maximum available reactive power, 6 - operating limit; active power insufficient to generate reactive power)

.

Test 3: Response to a request for manual control during Q(U) control at minimum active power

a) b)

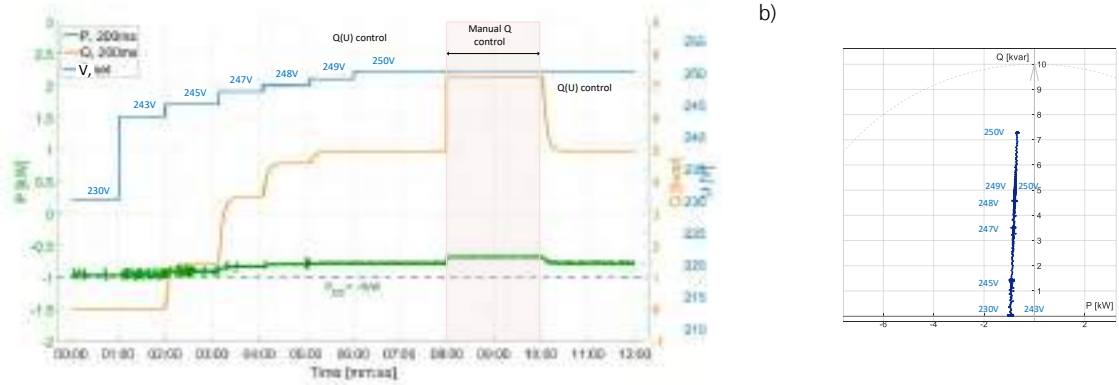

Figure 3.19. Output active and reactive power of PV inverter in response to voltage levels for a source power of 10% Pinstalled: a) time response b) PQ plane (Q(U) control mode based on the response curve → switch to manual control → return to Q(U) control mode)

.

Test 4: Response to a request for manual control during Q(U) control at maximum active power

a) b)

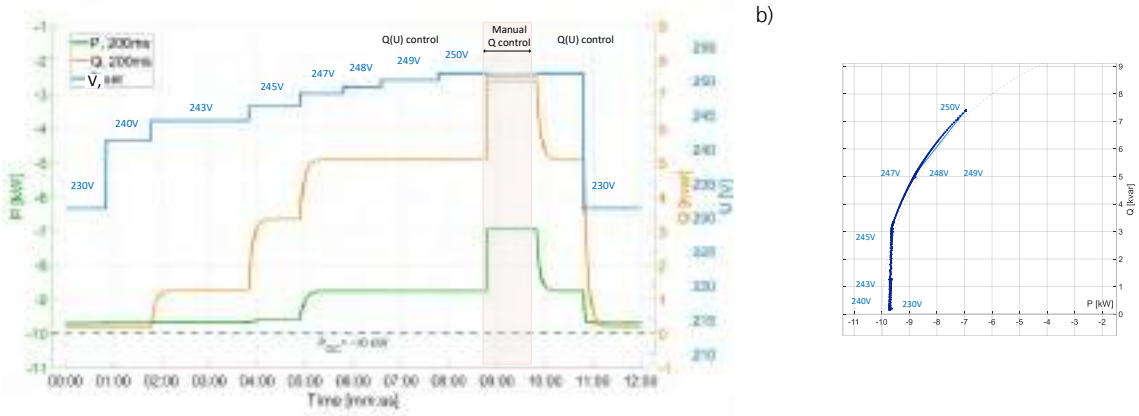

Figure 3.20. Output active and reactive power of PV inverter during reactive power request in response to voltage levels for a source power of 100% Pinstalled: a) time response b) PQ plane (Q(U) control mode based on the response curve → switch to manual control → return to Q(U) control mode)

.

Test summary in point of the reactive power regulatory potential of PV inverter:

- The 10 kW photovoltaic inverter provides 7.4 kvar of reactive power on demand.
- This capacity is available when the power available from the sun ranges from 10 kW to 0.2 kW.
- Access to reactive power is immediate, with no inertia.
- When Q(U) control mode is active, once the control curve is saturated (i.e. for voltages above 250 V), the inverter responds to a request for 7.14 kvar of reactive power, as referred to cosϕ=0.7
- Upon exiting manual control, the inverter smoothly returns to Q(U) control.
- The inverter's response to switching from automatic to manual control is effective for both the maximum and minimum required active power on the generator.

3.5.3 Mathematical Formulation and Optimization Framework

The objective of the proposed framework is to determine the optimal operating setpoints of distributed photovoltaic (PV) inverters in a low-voltage distribution network, such that voltage constraints are satisfied while minimizing active power curtailment and maximizing renewable energy utilization. The formulation integrates steady-state power flow modelling, a local inverter-control benchmark, and a centralized optimal power flow (OPF) problem for coordinated active and reactive power dispatch.

Let the distribution network consist of N buses, among which a subset $N_{PV} \subseteq N$ represents photovoltaic nodes. At each time step k, the available PV power is defined as:

$$P_i^{avail}(k) = \alpha(k)\, P_i^{rated} \tag{19}$$

where:

- $\alpha(k) \in [0,1]$ is the PV availability factor,
- P_i^{rated} is the installed PV capacity at bus i.

The decision variables of the optimization problem are:

$$x = \{P_i, Q_i\} \tag{20}$$

representing the active (P_i) and reactive power (Q_i) setpoints of PV inverters. The primary objective is to minimize total curtailment, expressed as:

$$\min \sum_{i \in \mathcal{N}_{PV}} \left(P_i^{avail} - P_i\right) \tag{21}$$

This formulation ensures maximum utilization of available renewable generation while respecting system constraints. The network must satisfy nonlinear AC power flow equations:

$$S_i = P_i + jQ_i = V_i \sum_{j=1}^{N} Y_{ij} V_j^* \tag{22}$$

where:

- V_i is the complex voltage at bus i,
- Y_{ij} is the admittance matrix.

Operation constraints are defined as follows. Voltage limits:

$$V_{min} \leq |V_i| \leq V_{max} \tag{23}$$

Generation limits (active and reactive power):

$$P_i^{min} \leq P_i \leq \min\left(P_i^{\text{avail}}, P_i^{max}\right) \tag{24}$$

$$Q_i^{min} \leq Q_i \leq Q_i^{max} \tag{25}$$

Inverter capability constraints:
The apparent power of each inverter is limited by (26). This constraint captures the physical capability of inverter hardware.

$$P_i^2 + Q_i^2 \leq (S_i^{max})^2 \tag{26}$$

3.5.4 Case study: Standard low voltage distribution network

The case study is based on a radial low-voltage distribution network representative of a Polish residential feeder. The system is supplied from an external 15 kV grid through a 15/0.4 kV, 630 kVA transformer. The downstream 0.4 kV network is arranged into two main feeder sections, denoted as Street A and Street B, which are further divided into four lateral branches: A-East, A-West, B-East, and B-West.
The network contains 52 residential prosumer connection points, labelled D01–D52. Each prosumer is connected to the nearest feeder node through a 25 m house service cable. The main feeder sections are modelled using YKY 4×70 Cu cables, while the lateral branches are modelled using YKY 4×25 Cu cables. Individual household connections are represented using WLZ YKY 5×10 Cu cables.
The external grid is represented by a short-circuit power of 250 MVA with equivalent resistance and reactance parameters. Cable parameters include resistance, reactance, susceptance, and thermal capacity limits. This structure provides a suitable test system for analysing voltage rise, reverse power flow, and the coordinated use of PV inverter active and reactive power in a high-PV-penetration residential LV network.

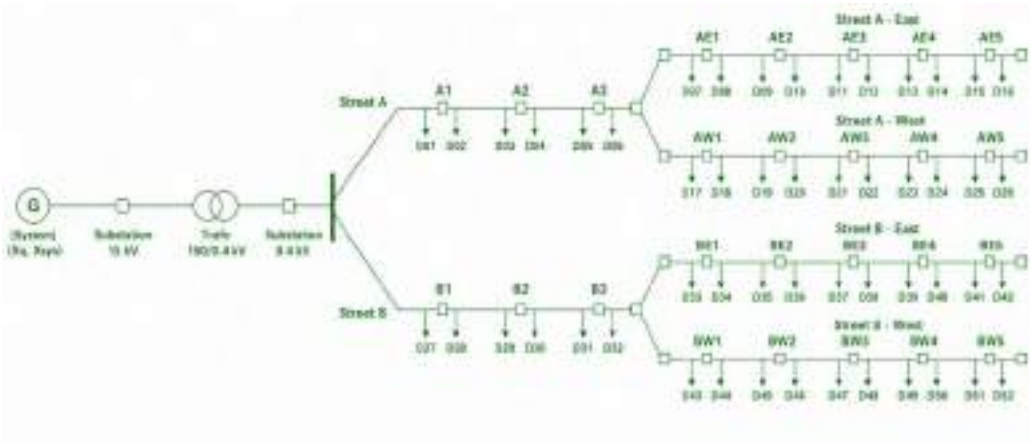

Figure 3.21. Polish radial low-voltage distribution network

3.5.5 Results (case study)

The proposed control strategies are evaluated on the considered radial low-voltage feeder under peak PV generation conditions for two inverter operating limits defined by minimum power factor constraints of cos ϕ = 0.7 and cos ϕ = 0.9. In both cases, the baseline operation characterized by unity power factor and no reactive support results in significant voltage violations, with a maximum voltage of 1.1328 p.u. and 30 buses exceeding the admissible limit. This confirms the limited hosting capacity of the network under uncontrolled PV injection.

For cos ϕ =0.7, the increased reactive power capability enables stronger voltage regulation. The local control strategy achieves a total active power injection of 301.6 kW with reactive consumption of –92.9 kVAr. The centralized OPF fully utilizes the available PV generation, reaching 339.0 kW, corresponding to 100% utilization, while employing –209.8 kVAr of reactive power. This represents a significant improvement in active power injection compared to local control, enabled by coordinated reactive power dispatch across all inverters.

For cos ϕ =0.9, the reduced reactive capability limits voltage support. While local control performance remains unchanged (301.6 kW, –92.9 kVAr), the OPF solution achieves 332.1 kW with –162.5 kVAr, indicating a reduced ability to exploit full PV availability compared to the cos ϕ = 0.7 case.

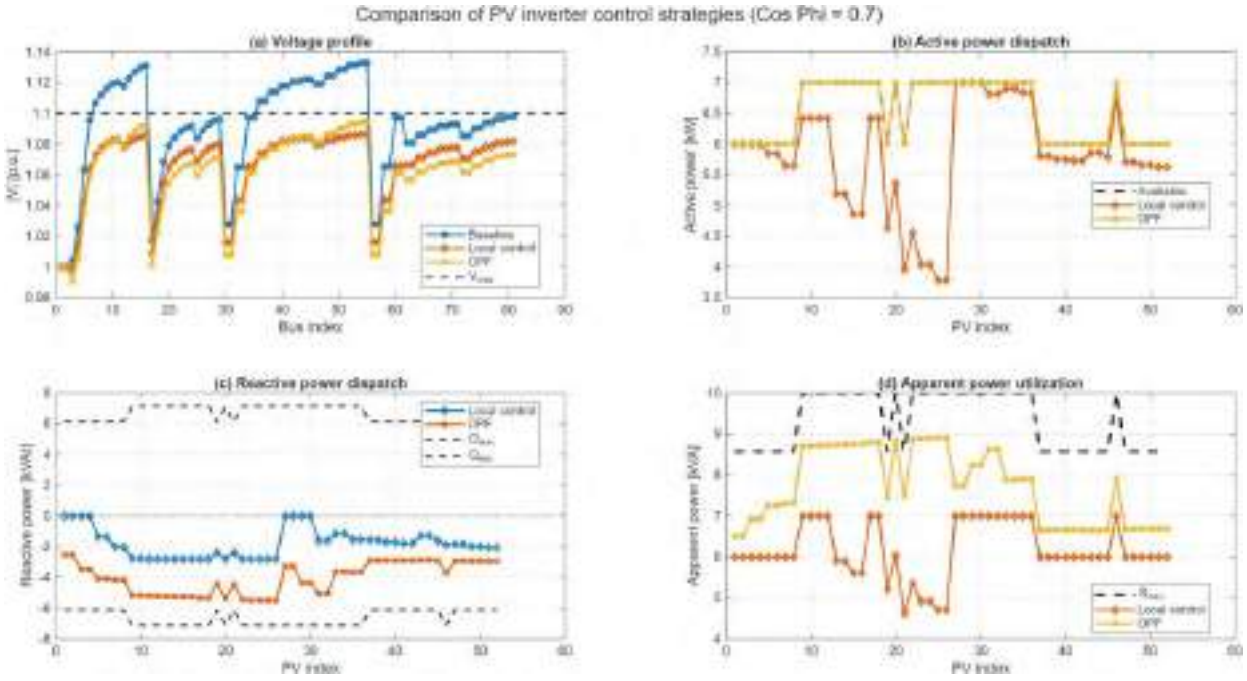

Figure 3.22. Comparison of PV inverter control strategies for cos ϕ = 0.7

Figure 3.22 presents the behaviour of the distribution network under three control strategies which are baseline, local control, and centralized OPF, when enhanced inverter flexibility is available (cos ϕ =0.7).

In (a), the baseline case exhibits significant overvoltage across multiple buses, clearly exceeding the 1.10 p.u. limit. The local control strategy partially mitigates this issue by absorbing reactive power, leading to a noticeable voltage reduction. The OPF further improves voltage regulation by coordinating all inverters, achieving the lowest overall voltage profile, although some buses still operate close to the upper limit due to network constraints.

In (b), local control reduces active power output for several PV units to maintain voltage within acceptable bounds, resulting in curtailment. In contrast, the OPF maintains generation close to the available maximum for all units, demonstrating its ability to minimize curtailment through coordinated reactive power support.

In (c), reactive power behaviour highlights the key difference between strategies. Local control provides moderate and spatially limited reactive power absorption based on local voltage measurements. The OPF, however, utilizes a significantly larger portion of the available reactive power range across multiple units, often operating near the inverter limits, thereby achieving system-level voltage regulation. In (d), the apparent power utilization confirms this observation: under OPF, many inverters operate closer to their apparent power limits (Smax), indicating efficient use of inverter capacity compared to local control which underutilizes available capacity due to its decentralized nature. Overall, the figure demonstrates that increased reactive power flexibility combined with centralized coordination enables higher PV utilization, reduced curtailment, and improved voltage regulation across the network.

Figure 3.23 presents the behaviour of the distribution network under three control strategies which are baseline, local control, and centralized OPF, when enhanced inverter flexibility is available (cos ϕ =0.9).

In (a), the baseline case again exhibits significant overvoltage, exceeding the 1.10 p.u. limit at multiple buses. The local control strategy reduces voltages through reactive power absorption, but the improvement is less pronounced compared to the cos ϕ =0.7 case due to tighter reactive power limits. The OPF achieves the best voltage regulation among the three strategies; however, voltage profiles remain closer to the upper limit, highlighting the reduced capability to control voltages under constrained inverter operation.

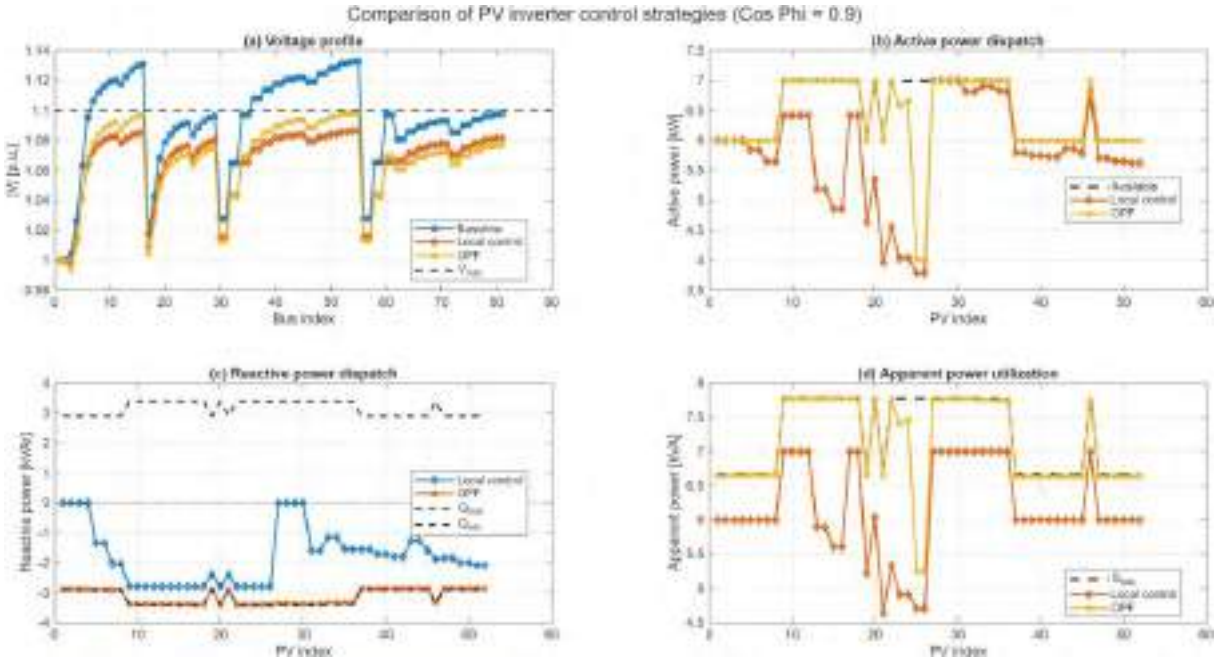

Figure 3.23. Comparison of PV inverter control strategies for cos ϕ = 0.9

In (b), local control leads to notable active power curtailment to maintain voltage within limits. The OPF improves active power utilization compared to local control, but unlike the cos ϕ = 0.7 case, it is unable to fully exploit the available generation. This reflects the direct impact of reduced reactive power flexibility on curtailment levels.

In (c), the reactive power dispatch is significantly limited. Both local control and OPF operate within a narrower reactive power range, with OPF still utilizing the available capability more effectively. However, the overall magnitude of reactive power support is visibly lower compared to the higher flexibility case. In (d), the apparent power utilization confirms these observations. Inverters under OPF operate closer to their reduced apparent power limits, but the overall utilization is lower than in the cos ϕ = 0.7 scenario. Local control again underutilizes available capacity due to its decentralized nature. Overall, the figure demonstrates that reduced inverter flexibility directly limits voltage control capability and increases curtailment. While centralized OPF still

outperforms local control, its effectiveness is constrained, emphasizing the importance of inverter capability in maximizing PV hosting capacity.

3.6 Advanced energy storage systems to enhance grid flexibility

3.6.1 Hydrogen technologies

The content of this section and the next one on hydrogen conversion technologies is contributed by the University of Rome "Tor Vergata" (UniTOV) within FlexBIT Work Package 2 — Task T2.8 ("Developing novel hydrogen technologies through detailed multiphysics modelling tools", led by UniTOV) and Task T2.6 ("Creating advanced energy storage systems to enhance grid flexibility"). It addresses the project's hydrogen pillar, formalized in FlexBIT functionality #11 Hydrogen as a Flexible Energy Carrier, whose goal is to bring High-Temperature PEM fuel cells in combined heat and power configuration to the residential sector, coupled with compact and safe on-site storage.
In the FlexBIT architecture, hydrogen plays two complementary roles. First, long-duration storage: the metal hydride bed described in §3.5.1.1, thermally buffered by the Phase Change Material jacket of §3.5.1.2, provides a low-pressure storage vessel that decouples renewable generation from community demand across seasonal time scales. Second, sector coupling: the HT-PEMFC described in §3.6 converts the stored hydrogen back into simultaneous electricity and high-temperature waste heat, at a thermal level directly usable by conventional domestic hot water and space heating distribution systems. The simulation tools reported below form the numerical backbone of this pillar. They have been developed and validated against reference data within WP2 and will be calibrated against the on-site experimental campaign of the UniTOV laboratory in WP3, supporting the TRL 4 → 6 step foreseen for the hydrogen technology track.

Seasonal variability of renewable energy sources introduces low-frequency fluctuations that short-duration storage technologies cannot address. Long-duration energy storage is therefore a necessary component of any high-renewables energy system. Hydrogen provides a viable pathway for this role: it can be produced via electrolysis during periods of excess generation and converted back to electricity or heat through fuel cells on demand.
Conventional hydrogen storage relies on high-pressure tanks, which entail significant compression energy and safety constraints. Metal Hydride (MH) storage and Phase Change Materials (PCM) thermal buffers represent technically mature alternatives that are directly applicable to stationary grid-connected applications.

3.6.1.1 Metal hydride hydrogen storage

MH tanks store hydrogen through reversible solid-state absorption by a metal alloy. Compared to compressed gas storage, they operate at significantly lower pressures (typically around 10 bar) and achieve higher volumetric energy densities, at the cost of reduced gravimetric capacity. These characteristics make them attractive for stationary installations where weight is not a primary constraint.
The main operational constraint of MH systems is thermal. Absorption is exothermic: the alloy temperature rises, which increases the equilibrium pressure (governed by the van't Hoff equation) until it matches the supply pressure and the reaction stalls. Desorption is endothermic: as hydrogen is released, temperature and equilibrium pressure drop; once the equilibrium pressure equals the user-side pressure, the reaction stops. In both cases, effective thermal management is essential to maintain practical charge and discharge rates.

Numerical modelling is a prerequisite for design and control of MH-based storage systems. It allows quantifying the coupled thermo-chemical dynamics, evaluating the impact of tank geometry and operating conditions, and screening thermal management configurations before hardware implementation.
A 1D numerical model of a cylindrical MH tank has been developed by University of Rome "Tor Vergata". The model resolves the coupled hydrogen charge/discharge dynamics and the thermal response of the storage system, providing a plant-level simulation tool for system sizing, thermal management design, and control strategy development. Details on the formulation and the numerical parameters are reported in [L. Bartolucci, E. Cennamo, S. Cordiner, V. Mulone, and A. Polimeni, "Hybrid Renewable Energy Systems: Integration of Urban Mobility Through Metal Hydrides Solution as an Enabling Technology for Increasing Self-Sufficiency," Energies, Oct. 2025, doi: https://doi.org/10.3390/en18195306].
The governing equations of the radial MH model cover thermodynamic equilibrium, reaction kinetics, and mass and energy conservation. The van't Hoff equation defines the equilibrium pressure of the hydride as a function

of temperature. Reaction kinetics follow an Arrhenius dependence on temperature with a pressure driving force relative to the equilibrium pressure; the overall reaction rate is modulated by the current alloy-density state, so that the reaction stalls as the bed approaches its saturation or depletion limit in the active direction.
Conservation equations close the model: hydrogen-mass conservation in the gas phase with Darcy-law transport through the hydride bed, solid-phase hydrogen balance driven by the reaction rate, and a combined-phase energy balance driven by a reaction heat source and by the net heat exchanged with the environment.

The tank interior is decomposed into four concentric domains: the metal hydride bed (MH), the gas-saturated porous region at the base of the bed (lower H_2 domain), the free hydrogen volume above (upper H_2 domain), and the steel tank wall (Tank domain). A schematic of this decomposition is reported in Figure . The MH, lower H_2 and Tank domains are each radially discretized; the upper H_2 domain is treated as a single lumped node under the assumption of spatially uniform gas properties. Node counts were determined through a sensitivity analysis on the model response to varied hydrogen demand profiles, selecting the coarsest discretization that preserved accuracy, to ensure computational efficiency suitable for integration into larger multi-physical simulation environments.
Each node is a concentric cylindrical control volume. Heat fluxes between adjacent nodes are computed from local thermal gradients and effective material properties. In the MH domain, effective thermal conductivity is evaluated as a porosity-weighted average of the hydrogen and alloy conductivities.

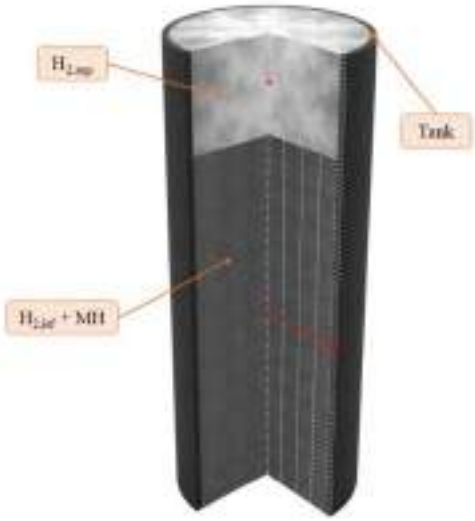

Figure 3.24. Domain discretization strategy adopted for the MH tank model. Red dots indicate node positions. Image from [L. Bartolucci, E. Cennamo, S. Cordiner, V. K. Krastev, V. Mulone, and A. Polimeni, "Metal Hydrides-Based Hydrogen Storage for Light Mobility Applications: Performance Assessment through 1D Numerical Modeling," J. Phys.: Conf. Ser., vol. 3143, no. 1, p. 012076, Dec. 2025, doi: 10.1088/1742-6596/3143/1/012076].

Thermal boundary conditions are applied at the outer tank wall to represent different heat exchange configurations.
The MH model has been validated against the 2D CFD reference of Chung and Ho [C. A. Chung and C.-J. Ho, "Thermal–fluid behavior of the hydrating and dehydriding processes in a metal hydride hydrogen storage canister," International Journal of Hydrogen Energy, vol. 34, no. 10, pp. 4351–4364, 2009, doi: 10.1016/j.ijhydene.2009.03.028], itself calibrated on the experimental dataset of Jemni et al. [A. Jemni, S. B. Nasrallah, and J. Lamloumi, "Experimental and theoretical study of a metal-hydrogen reactor"]; reproduction is obtained in close agreement with the reference data over the full parameter range in both absorption and desorption. Detailed validation figures of merit are reported in [L. Bartolucci, E. Cennamo, S. Cordiner, V. Mulone, and A. Polimeni, "Hybrid Renewable Energy Systems: Integration of Urban Mobility Through Metal Hydrides Solution as an Enabling Technology for Increasing Self-Sufficiency," Energies, Oct. 2025, doi: https://doi.org/10.3390/en18195306].

3.6.1.2 Phase Change Materials

The exothermic nature of hydrogen absorption and the endothermic nature of desorption make thermal management the dominant limitation of metal hydride storage. If the heat of reaction is not removed during charging, the bed temperature rises, the equilibrium pressure climbs to the supply pressure and absorption stalls; conversely, during discharging, the endothermic reaction cools the bed, the equilibrium pressure drops below the user-side pressure and hydrogen delivery fails. An active thermal management loop (pumped coolant, heat exchanger, controller) addresses this, but adds auxiliary power consumption, moving parts and control complexity that are difficult to justify in a stationary residential setting.

Phase Change Materials (PCM) provide a passive alternative. A PCM jacket placed in thermal contact with the hydride bed absorbs the reaction heat as latent heat during melting (charging) and returns it during solidification (discharging), matching the nearly isothermal character of the MH reaction and removing the need for an external heat sink during steady-state cycling. This simplifies the balance-of-plant, reduces parasitic consumption and improves the overall reliability of the storage unit.

A 1-D numerical model of the PCM jacket surrounding the MH tank has been developed by University of Rome "Tor Vergata" and validated against reference data. The formulation covers transient radial heat conduction in the PCM layer, latent heat effects during phase change through the enthalpy method, and thermal coupling with the MH domain.

Three different phase change materials are considered in the analysis: lithium nitrate trihydrate (LiNO3-3H2O, denoted as PCM1), the commercial salt hydrate SP29 (PCM2), and the paraffin-based material RT28HC (PCM3). The PCM model shares the same 1-D radial finite-volume framework as the MH domain, ensuring thermodynamic consistency at the MH–PCM interface and coherent numerical coupling.

The 1D radial finite-volume formulation follows the approach of Bartolucci and Krastev 2022 [L. Bartolucci and V. K. Krastev, "On the Thermal Integration of Metal Hydrides with Phase Change Materials: Numerical Simulation Developments towards Advanced Designs," Conf. Sustainable Mobility, Catania, Italy, Sep. 2022, pp. 2022-24–0018, doi: 10.4271/2022-24-0018]; axial heat transfer, natural convection in the molten PCM and buoyancy effects are neglected — standard assumptions for cylindrical tanks with high height-to-diameter ratios where radial gradients dominate.

The PCM thermal response is governed by the transient energy equation in 1D radial cylindrical form:

$$\rho c_p^{eff} \frac{\partial T}{\partial t} = \frac{1}{r}\frac{\partial}{\partial r}\left(r\lambda \frac{\partial T}{\partial r}\right) \tag{27}$$

where T the PCM local temperature, λ the effective thermal conductivity, and ρc_p^{eff} is the effective volumetric heat capacity, combining sensible storage and latent heat.

Using the enthalpy method, phase change is captured through a liquid fraction f_L that varies linearly from 0 (solid) to 1 (liquid) across a finite melting interval ΔT_m centeT_m.

The effective volumetric heat capacity combines sensible and latent contributions:

$$\rho c_p^{eff} = \rho_{avg}\left[(1 - f_L)c_{p,s} + f_L c_{p,l}\right] + \rho_{avg} L_m \frac{dfL}{dT} \tag{28}$$

where $c_{p,s}$ and $c_{p,l}$ are the solid- and liquid-phase specific heats, L_m the latent heat of fusion, and ρ_{avg} the average PCM density.

The effective PCM thermal conductivity is interpolated linearly between the solid and liquid values using the liquid fraction f_L, so that the composite conductivity transitions smoothly across the melting interval.

PCM mass and volume for a given MH tank are obtained by matching the PCM latent capacity to the total MH reaction enthalpy released over one absorption cycle, assuming the full heat of reaction is absorbed by the PCM through the solid–liquid transition; the required mass and volume follow directly from the PCM latent heat and density.

The PCM annulus is discretized radially using the same finite-volume approach as the MH domain. Each control volume balances conductive fluxes at its inner and outer faces; the outermost node includes an optional convective boundary condition with the surroundings.

The PCM model is validated against the numerical results of Bartolucci and Krastev for a MH–PCM system during hydrogen absorption. The reference geometry and operating conditions are replicated: LaNi5 alloy,

uniform initial temperature of 293 K, charging pressure of 8 bar, and no separating wall between the MH bed and the PCM jacket, allowing direct conductive coupling.
The comparison focuses on key quantities such as hydrogen absorption dynamics and f_L evolution over time. The results, reported in Figure , show agreement with the reference data within 10% relative deviation for all three PCMs. The 1-D formulation accurately captures the thermal behavior of the MH–PCM system during phase change while maintaining computational efficiency suitable for system-level simulations.

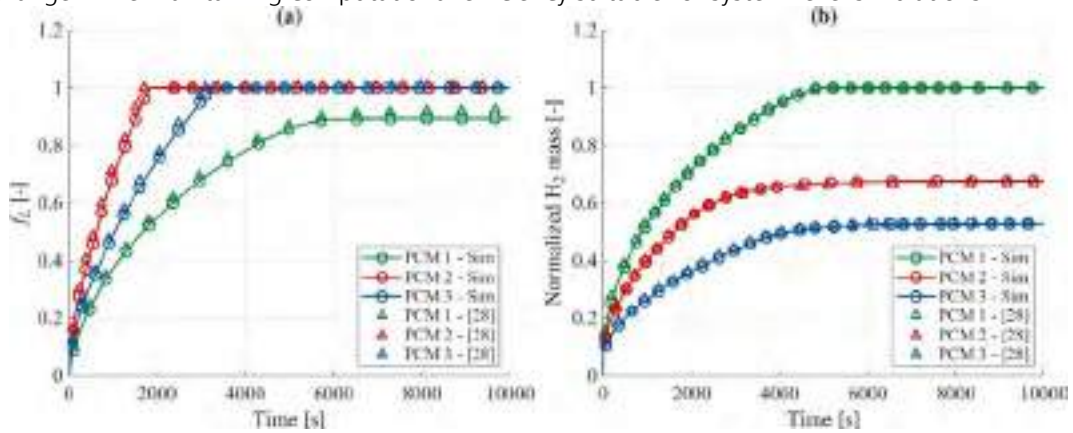

Figure 3.25. PCM model validation against reference data during hydrogen absorption. (a) Time evolution of the f_L for the MH system coupled with different PCMs. (b) Normalized absorbed hydrogen mass. Solid lines: simulation results; markers: reference data from [L. Bartolucci and V. K. Krastev, "On the Thermal Integration of Metal Hydrides with Phase Change Materials: Numerical Simulation Developments towards Advanced Designs," presented at the Conference on Sustainable Mobility, Catania, Italy, Sep. 2022, pp. 2022-24–0018. doi: 10.4271/2022-24-0018]. Image from [L. Bartolucci, E. Cennamo, S. Cordiner, V. K. Krastev, V. Mulone, and A. Polimeni, "Metal hydride-based hydrogen storage for fuel cell hybrid electric vehicles: numerical evaluation under real-world operating conditions," International Journal of Hydrogen Energy, vol. 231, p. 154877, May 2026, doi: 10.1016/j.ijhydene.2026.154877].

3.6.1.3 Integration of the hydrogen storage loop in a community-level Software-in-the-Loop platform

After being validated separately, the MH and PCM models have been integrated into a system-level simulation of the hydrogen loop of a renewable energy community, covering a full week behavior. The hydrogen pillar of the project consists of the complete chain composed by electrolyzer, metal hydride storage, and fuel cells: its behavior emerges only when the components operate together under realistic renewable-generation and load profiles, and the purpose of this section is to run the MH model at the community scale, driven by the same MPC controller that will supervise the demonstrator in WP3.

The simulation represents: a local plant hosting a photovoltaic array, a Proton Exchange Membrane Water Electrolyzer (PEMWE) and a metal-hydride tank bank (thermally managed by PCM jackets), complemented by two smart prosumers each carrying PV generation, a Battery Electric Storage System (BESS), a PEM Fuel Cell (PEMFC), a household load and a grid connection, plus one pure consumer carrying only a household load. All the community members are connected through the low-voltage bus; hydrogen is produced at the local plant, buffered in the MH bank and delivered to the prosumers' fuel cells on demand as electricity.

System operation is managed by a two-level hierarchical Model-Predictive Control (MPC) architecture. At the lower level, each community member runs its own local optimizer — one instance for the local plant (LP, managing PV + PEMWE + MH bank), one for each smart prosumer (SP1, SP2, managing PV + BESS + PEMFC) and one for the pure consumer. Every local optimizer solves a Mixed-Integer Linear Program (MILP, CVXPY + Gurobi) on a rolling 48-hour horizon with 15-minute timestep, using local PV and load forecasts and the latest plant state (BESS SoC, MH H_2 inventory, FC mass flow) pushed up from the Speedgoat real-time simulator. In a first pass, each local solves an unconstrained MILP and emits a flexibility bid to the upper level: the preferred net grid-exchange profile together with a feasibility envelope (minimum and maximum admissible exchange) and a marginal cost, derived from the operating limits of the local assets — C-rate, SoC bounds, fuel-cell ramp, electrolyzer turndown, MH headroom. At the upper level, the central coordinator aggregates the bids from all members and solves a community-level Quadratic Program that minimizes the aggregate community-to-grid exchange while penalizing the deviation of each member from its own preferred profile, subject to the per-

member feasibility envelopes and the connection limit of the community POD. The coordinator returns a per-member power target that maximizes community self-consumption without overriding the physical limits declared by the locals. Each local then re-solves its MILP with the received community target enforced as an equality constraint on the first timestep, producing the actual setpoints — BESS charge/discharge, electrolyzer stack power, fuel-cell dispatch, PV curtailment — that are returned to the Speedgoat through a Raspberry Pi CAN-to-MQTT bridge. All inter-controller communications travel on a publish/subscribe MQTT layer over a TLS-secured broker: each local publishes its bid on a dedicated uplink topic and subscribes to its own downlink topic for the community target, while the coordinator subscribes to the aggregated bid feed and publishes the per-member targets back; high-reliability QoS is used on the state and bid channels and a lower QoS on the high-rate telemetry. The link with the real-time plant uses CAN at 500 kbps between the Speedgoat and each Raspberry Pi, where the bridge maps the binary signals onto the corresponding MQTT topics. A side-channel of the coordinator broadcasts the community-wide H_2 availability published by the LP, so each prosumer caps its fuel-cell dispatch on the actual inventory of the shared MH bank, closing the hydrogen loop across the community.

The sizing adopted considers a residential-scale balance: the PEMWE nominal power (20 kW) is matched to the peak PV generation at the local plant so that all surplus generation can be converted to hydrogen; the MH storage capacity of 5.4 kg is matched to a few-days autonomy at the aggregated fuel-cell nominal power of the two prosumers (~ 1.5 kW each); the prosumers' BESS (5.2 kWh) covers intraday fluctuations, decoupled in time from the hydrogen route.

A first view of the community-level hydrogen loop is given in Figure , which reports both sides of the buffer over the full simulated week. The upper panel compares the instantaneous electrolyzer power at the local plant with the aggregated fuel-cell demand of the two prosumers: the PV-driven electrolyzer production clusters around the daylight hours with 6–8 kW peaks, while the fuel-cell demand appears mainly in the evening and morning with 2–3 kW peaks (to cover high user load demands together with the BESS). The lower panel shows the MH bank State of Charge (SoC), which oscillates in a 40–75 % band with a dominant daily period and a slower weekly drift.

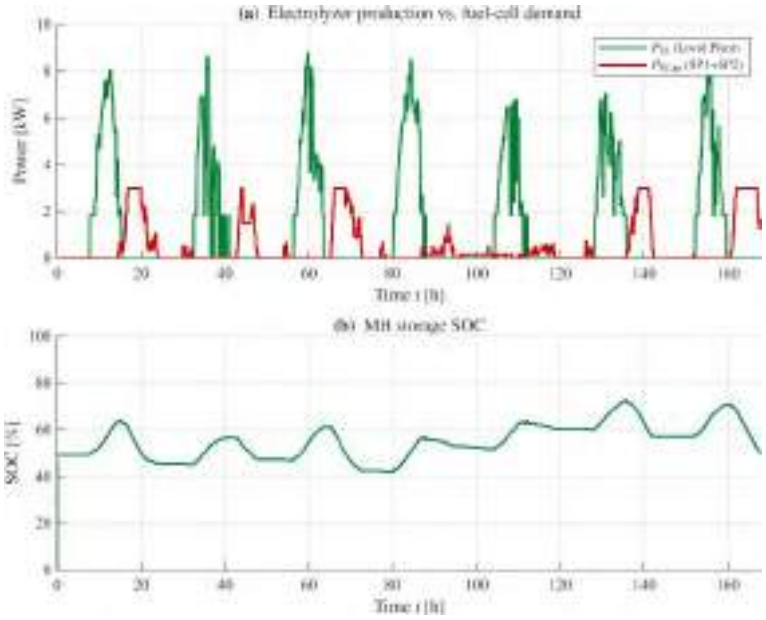

Figure 3.26. Community hydrogen loops over one representative week: (a) Instantaneous electrolyzer power at the local plant against the aggregated prosumer fuel-cell demand; (b) MH bank SOC.

As the absorption reaction is exothermic and the desorption reaction is endothermic, in limiting conditions, data on the thermal behavior have a key impact on the reaction itself. Thus, a closer look at the MH bank behavior is given in Figure , showing the ability of the bank to attend the hydrogen mass-flow setpoint as stated by the MPC.

In Figure the thermal behavior of metal hydrides confirms that the bed operates in a narrow 5° band between 27–32 °C. This assures that the bed operates comfortably into the operating envelope of the alloy, thanks to the PCM contribution as a thermal buffer.

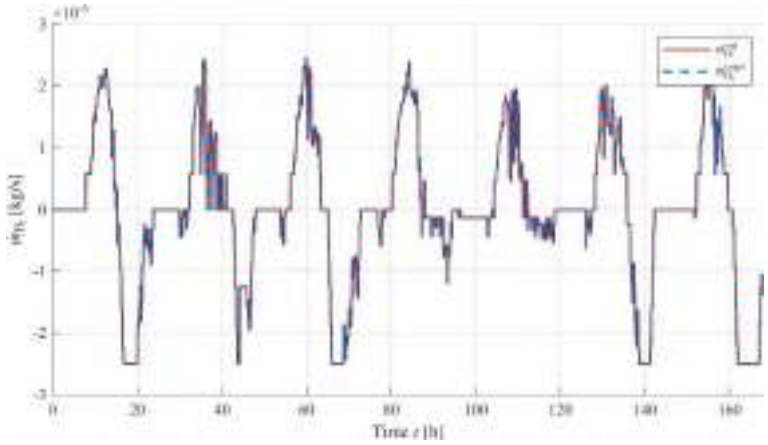

Figure 3.27. Comparison between the target and real hydrogen mass flow rate through metal hydride vessels.

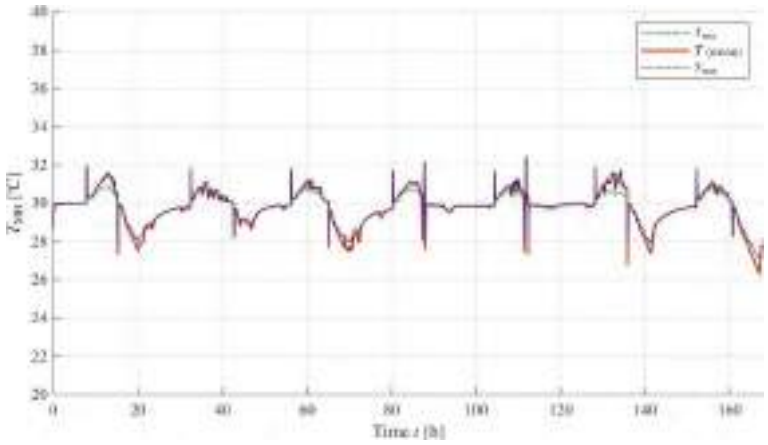

Figure 3.28. Radial envelope of the MH-bed temperature over the simulated week.

Overall, the community-scale simulation closes the chain from the component-level validation to the system-level operation, with MH and PCM models calibrated running coherently inside the community hydrogen loop.

3.7 Hydrogen conversion

Hydrogen electrochemical technologies convert hydrogen previously stored (§3.5.1) into the electrical and thermal energy carriers that community members can directly use with zero environmental impact while maximizing flexibility performance parameters.
Among the available fuel cell technologies, High-Temperature Proton Exchange Membrane Fuel Cells (HT-PEMFC) based on phosphoric-acid-doped polybenzimidazole (PA/PBI) membranes are particularly suited to residential combined heat and power (CHP) applications. Operation in the 120–200 °C range removes the need for liquid water management, raises tolerance to fuel impurities, and produces waste heat at a temperature level that is directly usable by conventional domestic thermal distribution systems. Against this background, a detailed HT-PEMFC stack model has been developed and validated.

3.7.1 HT-PEMFC Stack

HT-PEMFC cells store the electrochemical reaction heat in the membrane–electrode assembly (MEA) instead of generating liquid water: the PA/PBI membrane remains a dry proton conductor over the entire operating range, and the by-product water leaves the cell as vapor.
The main operational constraint is thermal. Proton conductivity of PA-doped PBI is a strong function of temperature: the stack cannot produce appreciable power until a minimum operating temperature is reached.

Once hot, the stack must be kept within a narrow window around its design point to protect the membrane from phosphoric acid leaching at high temperature and to avoid condensation at low temperature. Thermal management is therefore key to the optimal electrochemical operation, and any system-level model must resolve both domains in a coupled way.

The stack is represented as a set of cells connected in electrical series. The cell terminal voltage is obtained from the Nernst open-circuit voltage, where activation, ohmic and concentration overpotentials are subtracted. The stack voltage and power relate by linear scaling to the number of cells and the active area:

$$\begin{gathered} V_{cell} = E_{OCV} - \eta_{act} - \eta_{ohm} - \eta_{conc} \\ V_{stack} = n_{cells}\, V_{cell} \\ P_{stack} = V_{stack}\, I_{stack} \end{gathered} \tag{29}$$

where V_{cell} is the cell voltage, E_{OCV} the Nernst open-circuit voltage, and η_{act}, η_{ohm}, η_{conc} the activation, ohmic, and concentration overpotentials, respectively; V_{stack} and P_{stack} are the stack-level voltage and power; n_{cells} is the number of cells in series and I_{stack} the stack current.
The Nernst open-circuit voltage is written as:

$$E_{OCV} = E_0(T) + \frac{RT}{2F} \ln\left(\frac{p_{H_2}\, p_{O_2}^{0.5}}{p_{H_2O}}\right) \tag{30}$$

where $E_0(T)$ is the temperature-dependent standard electrode potential, R the universal gas constant, F the Faraday constant, and p_{H_2}, p_{O_2}, p_{H_2O} the partial pressures of hydrogen, oxygen, and water vapor in the electrodes. The standard potential is linearized around 298.15 K for gaseous product water:

$$E_0(T) = 1.185 - 2.302 \times 10^{-4}\,(T - 298.15) \tag{31}$$

Activation losses are evaluated separately for the oxygen-reduction reaction (ORR) at the cathode and for the hydrogen-oxidation reaction (HOR) at the anode through a Tafel formulation:

$$\eta_{act} = \frac{RT}{\alpha\, 2F} \ln\left(\frac{i + i_{leak}}{i_0(T)}\right) \tag{32}$$

where i is the local current density, i_{leak} the internal crossover current, α the charge-transfer coefficient and $i_0(T)$ the exchange current density at the operating temperature. Crossover is modelled as a constant current leak across the membrane. The exchange current density follows an Arrhenius dependence on temperature:

$$i_0(T) = i_{0,ref}\, \exp\left[-\frac{E_{act}}{R}\left(\frac{1}{T} - \frac{1}{T_{ref}}\right)\right] \tag{33}$$

with $i_{0,ref}$ the exchange current density at the reference temperature T_{ref} and E_{act} the activation energy of the corresponding electrochemical reaction. Since the hydrogen oxidation reaction on Pt/C in phosphoric acid is orders of magnitude faster than the oxygen reduction reaction, the cathode activation loss dominates the overpotential of the cell; default kinetic parameters (reference exchange current density, activation energy, transfer coefficient) are taken within the ranges commonly reported for HT-PEMFC PA/PBI MEAs and are subsequently refined by parameter identification against the experimental dataset described in the validation section.
Ohmic losses combine proton transport through the membrane and electronic/contact resistance of the plates and interfaces:

$$\eta_{ohm} = \left(\frac{t_{mem}}{\sigma_{mem}(T, DL)} + R_{contact}\right)(i + i_{leak})$$

(34)

where t_{mem} is the membrane thickness, $\sigma_{mem}(T, DL)$ the proton conductivity of the PA-doped PBI membrane and $R_{contact}$ a lumped area-specific resistance accounting for bipolar plates, current collectors, and interface contacts. Proton conductivity is described by an Arrhenius-type correlation in temperature and doping level:

$$\sigma_{mem} = 39.16\, DL\, \exp\left(-\frac{30964}{RT}\right) \tag{35}$$

where DL is the phosphoric acid doping level (mol H3PO4 per PBI repeat unit).
Mass-transport limitations at the cathode are described through a logarithmic concentration overpotential:

$$\eta_{conc} = B_{conc}\, \ln\left(\frac{i_{L,eff}}{i_{L,eff} - (i + i_{leak})}\right) \tag{36}$$

where B_{conc} is an empirical coefficient and $i_{L,eff}$ the effective limiting current density. The latter scales the reference value $i_{L,ref}$ with the cathode stoichiometry, the cathode pressure and the operating temperature:

$$i_{L,eff} = i_L \cdot \frac{\lambda_{ca}}{\lambda_{ca,ref}} \cdot \frac{P_{ca}}{P_{ref}} \cdot \sqrt{\frac{T_{ref}}{T}} \tag{37}$$

with λ_{ca} the cathode stoichiometry, P_{ca} the cathode total pressure, T the operating temperature, and $\lambda_{ca,ref}$, P_{ref}, T_{ref} the corresponding reference conditions ($\lambda_{ca,ref} = 2.0$, $P_{ref} = 1$ atm, $T_{ref} = 433.15$ K). The first factor captures the first-order effect of air supply on cathode oxygen concentration; the pressure factor follows Fick's law ($i_L \propto p_{O_2}$, with p_{O_2} proportional to p_{ca}); the temperature factor is a lumped approximation of gas-phase diffusivity through the gas diffusion layer.
Hydrogen and air consumption are obtained from Faraday's law and from the cathode stoichiometry and returned by the electrochemical sub-model together with the cell and stack outputs. The electrochemical heat generation is computed from the difference between the thermo-neutral voltage of the reaction ($E_{th} = 1.254$ V, gaseous product water) and the actual cell voltage:

$$\dot{Q_{gen}} = n_{cells}\,(E_{th} - V_{cell})\, I_{stack} \tag{38}$$

The thermal sub-model is a lumped-capacitance energy balance on the stack volume:

$$m\, c_p\, \frac{dT_{stack}}{dt} = \dot{Q_{gen}} - \dot{Q_{cool}} - \dot{Q_{amb}} \tag{39}$$

where $m\, c_p$ is the stack lumped heat capacity, T_{stack} the bulk stack temperature, $\dot{Q_{gen}}$ the electrochemical heat source described above, $\dot{Q_{cool}}$ the heat removed by the cooling circuit, and $\dot{Q_{amb}}$ the heat lost to the ambient. The stack thermal capacitance is reconstructed bottom-up as the sum over all physical components (bipolar plates, gas diffusion layers, PA/PBI membrane, end plates, current collectors, tie-rod hardware). For each layer i the heat capacity contribution is computed as $(m\, c_p)_i = \rho_i\, t_i\, c_{p,i}\, A_{cell}\, f_{area,i}$, where the area factor $f_{area,i}$ accounts for manifolds, bolt holes and flow-field lands exceeding the active footprint; end plates use a larger area factor to account for the structural plates supporting the tie rods. Material properties are taken from standard mechanical engineering references.
Ambient heat losses are treated as a linearized convection-plus-radiation conductance over the stack external surfaces:

$$UA_{amb} = (h_{nat} + h_{rad})\, A_{ext}$$
$$h_{rad} = \varepsilon\, \sigma_{SB}\, (T_{stack} + T_{amb})(T_{stack}^2 + T_{amb}^2) \tag{40}$$

where h_{nat} is a natural-convection coefficient for a vertical plate in air at the stack surface temperature, h_{rad} is the linearized Stefan–Boltzmann radiation coefficient evaluated at the nominal operating temperature with surface emissivity $\varepsilon = 0.85$, and A_{ext} is the total external surface of the stack, computed from the stack length and the bipolar-plate footprint.
Heat removal from the stack is obtained through dedicated serpentine cooling plates interleaved with the cells. A diathermic fluid flows through the plates; the same fluid can be used for stack pre-heating. The cooling conductance is evaluated dynamically at every time step through a series resistance combining conduction through half of the bipolar-plate thickness and convection from the channel wall to the fluid:

$$\frac{1}{U_{cool}} = \underbrace{\frac{t_{BP}/2}{k_{BP}}}_{\text{conduction}} + \underbrace{\frac{1}{h_{cool}}}_{\text{convection}}$$
$$n_{cool} = \left\lfloor \frac{n_{cells}}{n_c} \right\rfloor$$
$$A_{cool} = 2\, n_{cool}\, A_{cell}$$
$$UA_{cool} = U_{cool}\, A_{cool} \tag{41}$$

where k_{BP} is the through-plane thermal conductivity of the bipolar plate, h_{cool} the convective heat transfer coefficient on the coolant side, and A_{cool} the total channel wall area (n_{cool} cooling plates, each with area A_{cell}, wetted perimeter P_{wet} and channel length computed from the serpentine layout).
The convective coefficient is obtained from the Nusselt number Nu, itself a function of the channel Reynolds number Re and Prandtl number Pr, and is updated dynamically according to the coolant mass flow rate set by the external controller.
The coolant outlet temperature and the heat removed from the stack are then obtained from an $\varepsilon - \mathrm{NTU}$ lumped-stack formulation with constant hot-side temperature:

$$\mathrm{NTU} = \frac{UA_{cool}}{\dot{m}_{cool}\, c_{p,cool}}$$
$$\varepsilon = 1 - e^{-\mathrm{NTU}}$$
$$T_{cool,out} = T_{cool,in} + \varepsilon \left(T_{stack} - T_{cool,in}\right)$$
$$\dot{Q}_{cool} = \dot{m}_{cool}\, c_{p,cool} \left(T_{cool,out} - T_{cool,in}\right) \tag{42}$$

where $\dot{m}_{cool}$ is the coolant mass flow rate, $c_{p,cool}$ its specific heat, $T_{cool,in}$ the coolant inlet temperature and T_{stack} the bulk stack temperature. Temperature regulation is then obtained by acting on $\dot{m}_{cool}$ (PID-controlled coolant pump) and, during start-up, on the coolant inlet temperature $T_{cool,in}$.

The HT-PEMFC model has been validated against the 3-D CFD results reported by *Krastev et al.* [V. K. Krastev, M. Baldelli, L. Bartolucci, F. Donato, M. Kheir Rouz, and V. Mulone, "Optimal cathode design of a single high temperature PEM fuel cell: A computational study," International Journal of Hydrogen Energy, vol. 142, pp. 80–89, Jun. 2025, doi: 10.1016/j.ijhydene.2025.05.346], obtained on a BASF Celtec P1100W PA/PBI membrane-electrode assembly under hydrogen/air operation at 160 °C and atmospheric pressure. Five CFD datasets corresponding to four cathode serpentine channel designs (D1–D4) are used for comparison.
The validation outputs comprise (i) a metrics table (Table) reporting, for each dataset, the RMSE, the maximum absolute error and the coefficient of determination R^2 of the modelled cell voltage; (ii) the polarization-curve comparison and residuals plots (Figure); and (iii) an overpotential-breakdown plot (Figure) that resolves the contribution of each loss mechanism — cathode activation, anode activation, ohmic and concentration — to the total overpotential of the cell.
Despite the lumped, zero-dimensional nature of the present model, the predicted polarization curves closely reproduce those of the spatially resolved 3-D CFD model, confirming that the semi-empirical formulation is able to capture the dominant electrochemical losses without requiring high computational costs typical of a full CFD simulation.

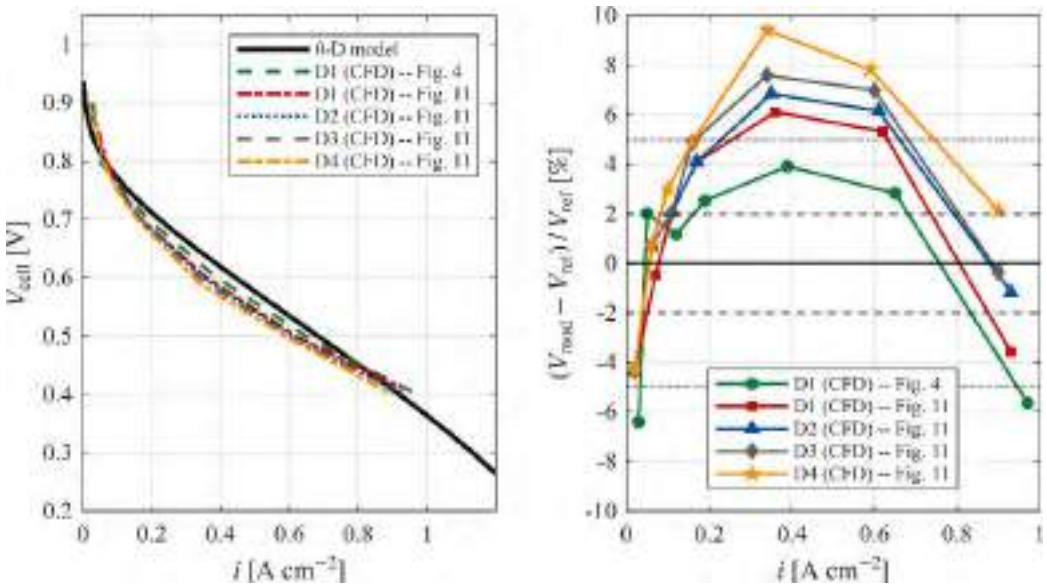

Figure 3.29. Comparison between the 0-D model and the Krastev et al. CFD results for four cathode channel designs (D1-D4). Left: experimental vs. modelled cell voltage; right: relative voltage error.

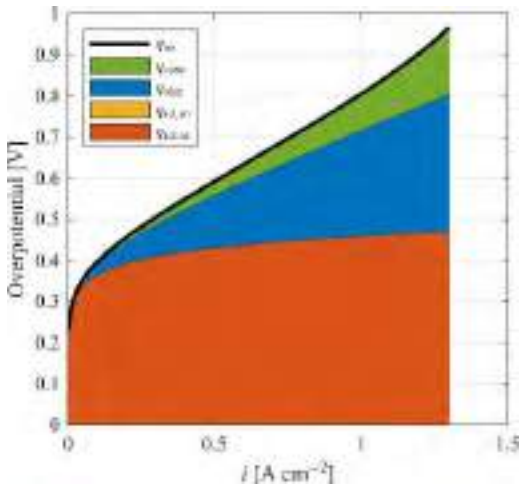

Figure 3.30. Overpotential breakdown of the HT-PEMFC cell as a function of current density at the nominal operating point (T = 160 °C, λ_{ca} = 2.0, λ_{an} = 1.2, atmospheric pressure).

Table 3.3. HT-PEMFC model validation metrics against the Krastev et al. CFD model.

Dataset	RMSE [mV]	RMSE [%]	MaxE [mV]	R^2
D1 (CFD) – Fig. 4	27.3	3.92	57.6	0.9715
D1 (CFD) – Fig. 11	26.3	4.11	38.9	0.9728
D2 (CFD) – Fig. 11	27.4	4.25	41.1	0.9713
D3 (CFD) – Fig. 11	29.9	4.69	45.5	0.9649
D4 (CFD) – Fig. 11	33.6	5.43	55.5	0.9572

3.8 Scenario-to-demonstrator mapping

Table 3.4. Scenario-to-demonstrator mapping

Demonstrator / Site	Country	REC	Flexibility/DR	Local balancing	Ancillary services
German industrial community (aRTE Möbel + Aue Bestattungen)	DE	Yes (community)	Yes	Yes	TBD
UNITOV HiL hydrogen pilot	IT	Yes (community simulation)	Yes	Yes	Simulated
UNIPA Smart Energy Parking	IT	Yes	Yes	Yes	Yes
Pantelleria solar cooling	IT	Possibly	Yes	TBD	TBD
Malta digital twin microgrid	MT	TBD	Yes	Yes	TBD
Electrum / Alu-Frost facility	PL	Yes	Yes	Yes	TBD
WUST demonstrator	PL	TBD	Yes	Yes	TBD

4 Functional Design of Energy Exchange Mechanisms

4.1 Self-Consumption and Community Energy Sharing

Self-consumption and community energy sharing are core FlexBIT mechanisms for increasing the local use of renewable generation and reducing unnecessary grid exchange. From a functional perspective, the mechanism must provide a common framework for measuring energy flows, defining the sharing perimeter, applying allocation rules, and storing transparent records for later verification and settlement. This is consistent with the FlexBIT objective of supporting self-consumption and coordinated energy exchange within energy communities through a common digital platform [1, 3].

The minimum required functions are the following:

- Consistent metering and measurement model: the system must represent power and energy in a uniform way at both asset and site level. This includes, where relevant, PV generation, BESS charge/discharge, EV charging, controllable loads, and site import/export values. A common measurement basis is necessary to determine how much energy is produced, consumed, stored, exported, or shared.

- Aggregation rules: the mechanism must define the operational perimeter within which energy sharing is evaluated. This includes:
    - the assets and members included in the site or community;
    - the boundary used for aggregation;
    - the time window over which production and consumption are matched.

  These rules are necessary to identify the amount of energy that can be considered locally shared.

- Allocation and sharing logic: once measurements are collected and aggregated, the system must apply a rule to assign shared energy to each participant. This allocation may depend on:
    - predefined participation criteria;
    - member profiles;
    - contractual or regulatory conditions;
    - community-specific sharing rules.

  At minimum, the mechanism must support a clear and reproducible allocation method for each accounting interval.

- Accounting records and traceability: the results of the sharing process must be stored in auditable records. These records should include:
    - measured and aggregated values;
    - applied allocation rules;
    - assigned shared energy values;
    - timestamps and relevant identifiers.

  This is necessary for transparency, verification, and possible settlement processes. FlexBIT also foresees traceability and secure logging as enabling functions of the wider platform architecture

4.2 Flexibility Activation and Congestion Management

Minimum required functions:

- flexibility description (power/time, constraints)
- dispatch plan generation (rule-based or optimization-based)
- dispatch output interface (format + delivery)

4.3 Local Balancing and Ancillary Services

Table 4.1. Local balancing and acillary services of demonstrators

Site	Telemetry resolution	Response time threshold	Controllable assets included
Germany aRTE Möbel	• Loads: 1 sec. • Battery: 1 sec. • Compressor: 1 sec. • EV charging station: 3 sec. • PV_ 10 sec.	In average 100 ms	Battery Compressed air Charging station
Germany Aue	• Loads: 10-15 sec. • Battery: 3 sec. • EV charging station: 3 sec. • PV: 3 sec.	In average 100 ms	Battery Charging station Cooling aggregators
Poland AluFrost	• Car Charger 1s • Battery charging station 1s • PV 1s	In average 100ms	Car Charger Battery charging station PV
Poland WUST LAB	• Load: 1 sec. • Battery: 1 sec • PV: 1 sec	In average 100ms	Loads Battery PV AC Grid simulator PV Array Simulator

4.4 Settlement and Accounting Principles

- Phase 1 (minimum): *kWh shared × allocation key* (per site/community)
- Phase 2 (extended): incorporate flexibility remuneration and market interaction (if applicable)

4.4.1 Germany: Industrial Energy Community

The German case study considers the sharing of electricity and flexibility between an industrial and a tertiary building. The two buildings are located approximately 800 meters apart and belong to the same balancing group (*Bilanzkreis*). The basic operational objective of both buildings is to function as Net-Zero, namely to maximize self-consumption while avoiding feeding electricity into the grid. In addition to this, a digital trust solution focused on the energy sustainability of the manufactured items of the industrial facility (aRTE Möbel) is considered. The digital trust aims to create transparency regarding the source of electricity used within the industrial system. Energy sustainability is therefore supported on one side through the self-generated electricity at the industrial facility, and on the other side, if necessary, through the electricity self-generated at the tertiary facility (Aue). The settlement for energy sharing between the two facilities will therefore be based on the added value that the digital trust creates for the industrial process.

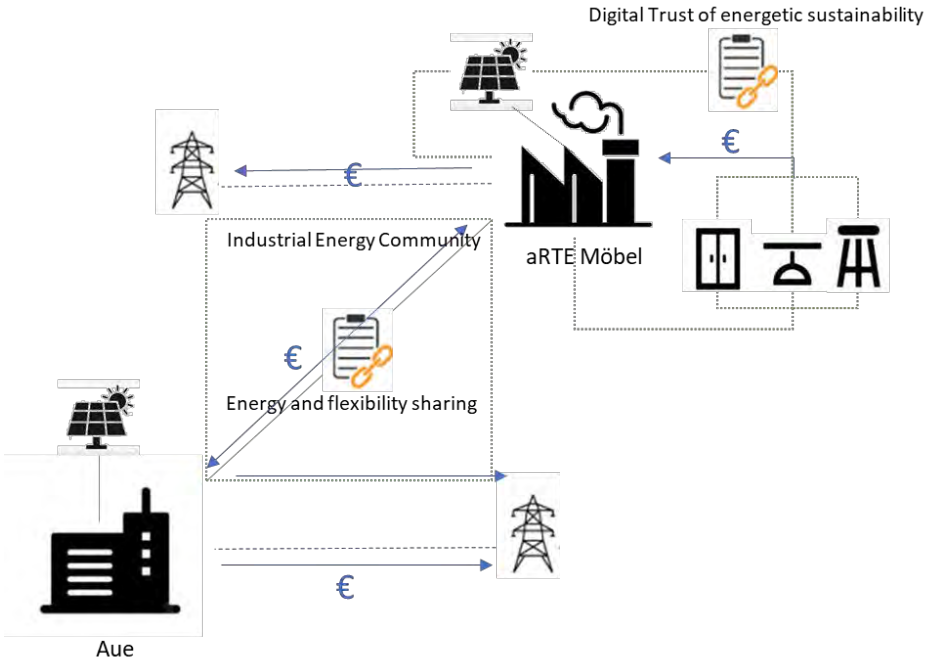

Figure 4.1 Industrial energy community in the German demonstrator

5 Centralized FlexBIT Platform: Implementation Status

This chapter summarizes the current implementation status of the centralized FlexBIT platform and connects it to the broader architecture defined at project level. The platform currently provides a unified API layer for demonstrator data, canonical signal normalization across heterogeneous sites, a blockchain-based data attestation layer, and partner-facing tools for verification and access. In this way, the implementation already reflects the main FlexBIT principle of coordinating heterogeneous demonstrators through a common digital environment while preserving site-level autonomy. For full architectural specifications, refer to D1.1.

5.1 Reference Architecture Overview

The current platform implementation follows the FlexBIT concept of centralized coordination over site-specific local control. At platform level, demonstrator data are exposed through a unified API that normalizes different internal field names into canonical fields shared across all sites. The device categories include BESS, EV chargers, PV, thermal systems, cooling aggregators, hydrogen, community controllers, demand, CAES, and grid metering, confirming that the architecture is organized around common functional layers rather than demonstrator-specific interfaces.

Accordingly, the architecture can still be described through the two-loop concept:

- Fast local loop – managed by pilot-specific systems such as SCADA, PLC, EMS, or equivalent local controllers;
- Slow advisory loop – coordinated by the centralized FlexBIT platform, which receives normalized data, supports cross-site coordination, and provides supervisory, monitoring, and verification functions.

5.2 Platform Interfaces and Monitoring

The FlexBIT platform currently exposes a unified API interface for accessing energy data from all demonstrators. Although each site uses different internal signal names and local technologies, the API translates them into canonical fields, allowing a common representation of the same quantities across sites. The API is organized by device category and includes dedicated endpoints for BESS, EV/V2G, PV, thermal systems, hydrogen, community controllers, demand, CAES, and grid metering. Authentication is handled through bearer tokens and API keys for metrics management and blockchain node managed setup.

At interface level, the current implementation includes:

- configuration and access through authenticated API services;
- category-based ingestion and status endpoints for the main FlexBIT asset classes;
- canonical signal normalization across heterogeneous demonstrators;
- structured alarm handling for diagnostics and supervision.

In addition to the currently available API services, the broader FlexBIT platform concept also foresees stakeholder-oriented interface views for external actors such as DSOs, energy suppliers, and market operators. These should be understood as part of the intended platform interaction model rather than as fully implemented interfaces at the current stage. Among these roles, the presently documented material already reflects the logic of external supervisory interaction, for example through the community control concept, while the complete stakeholder-facing views remain part of the planned platform evolution

5.3 Smart Contracts and Blockchain

The blockchain layer of the FlexBIT platform is designed to provide trust, immutability, and independent verifiability for the data managed by the platform [5]. Its role is not limited to future settlement functions but already includes a concrete data-attestation mechanism through which platform measurements and processing

results can be anchored on-chain and later verified by partners. In this way, the blockchain infrastructure supports the integrity of the FlexBIT ecosystem while reducing dependence on a single centralized trust point. FlexBIT uses a private Hyperledger Besu blockchain network with QBFT (Quorum Byzantine Fault Tolerance) consensus, and a node architecture including full nodes, validators, and partner nodes.

The current network design is based on a permissioned Ethereum-compatible infrastructure [6], which allows controlled participation by project actors while maintaining resilience through BFT consensus. In practice, this means that the network is suitable for a consortium setting such as FlexBIT, where trusted organizations need a shared and tamper-evident record without exposing all information to a public blockchain. The presence of dedicated partner nodes, which can independently verify on-chain attestations and optionally participate more actively in the network, further strengthens transparency across the consortium.

From a functional point of view, the blockchain layer supports the following main objectives:

- **network trust** and **resilience**, through a permissioned Besu infrastructure with QBFT consensus;
- **process automation**, through smart contracts used as trusted registries for attested platform data;
- **immutability** and **traceability**, through on-chain registration of data fingerprints and related metadata;
- **privacy preservation**, by keeping detailed operational datasets off-chain while anchoring only their cryptographic proofs on-chain;
- **independent verification**, by allowing partner nodes to check whether the data shown in the platform correspond to the originally attested records.

A key implementation concept is the separation between off-chain storage and on-chain attestation. The current documentation explicitly states that daily aggregated measurements are hashed into Merkle trees and recorded on-chain through smart contracts. The integrity flow is:

Telemetry → Kakfa → Data Processor → Smart Contract → On-chain Attestation.

This means that telemetry data are first ingested through Kafka, then processed and aggregated off-chain, after which a Merkle tree is computed over the dataset. The resulting Merkle root and the corresponding daily energy totals are written to the blockchain. This approach makes it possible to verify that a dataset has not been modified after registration, without storing the full raw dataset directly on-chain.

Within D2.1, this concept can be described as extending beyond daily aggregates toward a broader metric-level immutability model. The intended principle is that each metric managed by the platform can be represented through hashed data, so that any value displayed in the FlexBIT application can later be checked against its attested fingerprint. In this way, immutability is not limited to the aggregate result alone but can support verification of the integrity of the underlying records that contribute to the value shown on the platform. Technically, this is enabled by the Merkle-tree structure: individual records or metrics are hashed as leaves, combined into a tree, and anchored through the root registered on-chain. A later verification process can then demonstrate whether a single metric belongs to the attested dataset and whether it has remained unchanged. This is a direct extension of the currently documented Merkle-based attestation approach.

In practical terms, the blockchain and smart-contract layer can therefore be summarized through the following functions:

- **Network infrastructure**: deployment of a private Hyperledger Besu network with QBFT consensus to ensure controlled participation, fault tolerance, and consortium-level resilience [6].
- **Smart-contract registry**: use of smart contracts to register attested data fingerprints and related totals in a trusted and immutable way.
- **Immutability and traceability**: registration of hashed data and processing results on-chain, creating a tamper-evident historical record of platform-relevant measurements and decisions.
- **Privacy layer**: commercially sensitive or high-volume operational data remain off-chain, while only cryptographic proofs are stored on-chain. This preserves confidentiality and scalability while still enabling trustable verification.

- **Off-chain data integrity**: Merkle-proof anchoring enables later verification of off-chain datasets and, conceptually, of single metrics shown in the application, by checking them against the attested blockchain fingerprint.

At the current stage, it is safest to describe the implemented blockchain layer primarily as a data integrity and attestation framework.

5.4 Infrastructure Layer

5.4.1 Digital

The digital infrastructure of the FlexBIT platform is conceived as a cloud-oriented PaaS environment based on containerized microservices, orchestration tools, and automated deployment workflows. In the target architecture, this layer is intended to support scalability, modularity, controlled service deployment, and easier maintenance across the different platform components. The reference setup includes:

- **Docker microservices**, used to package platform services in isolated and portable containers;
- **Kubernetes orchestration**, intended to manage service deployment, scaling, resilience, and lifecycle management;

At the current stage of the project, however, this digital infrastructure is not yet deployed as a full production environment. The platform is currently operating in a testing environment, which is being used for development, integration, and validation of the main platform services and interfaces (WP3). Therefore, Kubernetes-based orchestration, and the full PaaS setup should be considered as the target deployment model, while the presently available environment mainly supports testing and pre-production activities.

This distinction is important because the current implementation status reflects an intermediate stage: the core software components and platform services are being developed and validated, but the final production infrastructure is still to be completed.

5.4.2 Energy assets

The following table shows the devices owned by every demonstrator.

Table 5.1. Devices owned by evey demonstrator

Demonstrator	Electricity generation	Energy storage Systems	Charging station	Controllable load
aRTE Möbel	Photovoltaic: 126 kW	• Battery: 20 kW; 20 kWh • Compressed air: 500 liter, 8 bar	2x11 kW	Industrial process (passive control)
Aue	Photovoltaic: 30 kW	• Battery: 20 kW, 20 kWh	3x 11 kW	Cooling aggregate
Alu Frost	Photovoltaic 300 kW	Battery: 172,5 kWh	50 kW 160 kW	Industrial process (passive control)
WUST LAB	PV inverter 10kW with 15kW Solar Array Simulator	Battery: 2.4kWh	-	1kW/1.2kvar controllable load
Unipa Smart Parking	PV inverter 2x20 kW – PV field 40 kW	Batteries: 54 kWh	2x10 kW	Lighting system; Charging stations
Unipa Solar cooling				Heat pump

6 Control, Optimization, and Decision Logic

6.1 Forecasting Inputs

The optimization layer relies on forecast outputs produced by the FlexBIT Forecasting Tool, whose full methodological description is provided in D2.2 (§2–4). Two forecasting domains are relevant in this context: solar/PV generation and load demand.
For solar generation, two parallel forecasting pipelines have been developed, both operating on a rolling 1-minute basis — meaning a new prediction is issued every minute, each time covering the 15 minutes ahead:

- **Architecture B (feature-based pipeline)** — draws on astronomical variables such as sun zenith and azimuth angles, geolocation parameters, and historical PV or irradiance measurements. Given its low computational footprint, this approach is well suited for edge deployment directly at demonstrator sites.
- **Architecture A (image-based pipeline)** — processes sky imagery through a Convolutional Neural Network for spatial feature extraction, combined with an LSTM network for temporal modeling, supplemented by historical PV output and astronomical features.

Both architectures are benchmarked against the SKIPP'D 15-minute ahead reference baseline.
For load demand forecasting, the methodology is currently under joint development by WUST, SRI PAS, and UNIPA and will be described in full in D2.2.
Forecast outputs — predicted PV generation values refreshed every minute — are consumed by the optimization layer on demand, alongside real-time asset states such as battery state of charge and hydrogen tank pressure where applicable. These operational states are sourced independently from the IoT Data Hub via MQTT and should not be confused with forecast outputs. The forecasting module itself is fed by historical data from EMACS SQL, real-time streams from the IoT Data Hub, and contextual metadata from SCADA systems, as described in D1.1 §[Data Analytics Platform].
Should forecasts become unavailable due to connectivity loss or model failure, the optimization layer falls back to the last known valid schedule or a safe rule-based policy, as described in §5.5.3.

6.2 Optimization Objectives and Constraints

The optimization layer defines the decision logic used by the FlexBIT platform to coordinate distributed flexibility resources across the demonstrators. Its main objective is to improve the operation of local energy systems by maximizing renewable energy self-consumption, reducing energy exchange with the external grid, supporting flexibility activation, and maintaining safe operation of local assets. Depending on the demonstrator configuration, the optimization may consider photovoltaic generation, site demand, BESS state of charge, EV/V2G availability, hydrogen storage status, thermal loads, compressed air systems, and other controllable resources.

The optimization process uses **forecasted PV generation** and **demand profiles**, together with real-time asset states collected through the platform interfaces. These inputs are used to generate schedules or advisory setpoints over a rolling horizon, typically with a minimum 15-minute time resolution. The objective function may combine technical and economic criteria, including minimization of grid imports, maximization of shared renewable energy, reduction of peak demand, minimization of curtailment, and preparation of flexibility margins for local balancing or flexibility-market participation.

The optimization problem is constrained by the physical and operational limits of each asset. For storage systems, constraints include minimum and maximum state of charge, maximum charge and discharge power, efficiency losses, and cycling limitations. For EV/V2G resources, user mobility requirements, vehicle availability, minimum departure state of charge, and maximum charging or discharging power must be respected. For controllable loads, flexibility windows, comfort limits, process constraints, and site-specific operational priorities are considered. In all cases, local safety rules and device-level protection mechanisms remain under the responsibility of the local control systems.

Examples of actions and rules for optimization flow can be found in Chapter 3 of this deliverable.

6.3 Dispatch and Control Strategy

The **dispatch** and **control strategy** translates optimization results into operational schedules, setpoints, or recommendations that can be applied by each demonstrator according to its technical capabilities. The FlexBIT platform does not replace local SCADA, EMS, PLC, or device-level controllers; it acts as a supervisory coordination layer. Local systems remain responsible for real-time execution, safety interlocks, asset protection, and immediate response to abnormal operating conditions.

Dispatch outputs may include battery charge/discharge profiles, EV charging or V2G activation windows, controllable-load modulation requests, hydrogen-system operating instructions, photovoltaic inverter setpoints, or flexibility availability signals. These outputs are typically structured using 15-minute intervals and may be generated over a rolling horizon, for example, 24 hours. The update cadence may vary between demonstrators, typically between 15 and 60 minutes, depending on communication availability, local control architecture, and the flexibility service considered. Dispatch instructions may be exchanged through API pull, where the local adaptation layer retrieves the latest schedule, or API push, where the platform sends updated instructions to the site. In both cases, the local controller validates the received instructions before implementation, checking asset availability, state of charge, device limits, user requirements, process constraints, and local safety thresholds.

A **degraded operating condition** occurs when the platform cannot generate or deliver an updated optimized dispatch schedule because one or more required inputs are unavailable, delayed, or fail validation. These inputs may include site measurements, asset-status data, PV or demand forecasts, market signals, or other contextual information required by the specific demonstrator. Weather forecasts are considered optional contextual inputs and are only relevant for sites or functions that use them for PV, thermal, or demand forecasting; individual pilot sites are not required to independently check weather conditions unless this is part of their local implementation.

When degraded mode is activated, the affected site continues operating under local responsibility. The local controller may temporarily apply the last valid dispatch schedule if it remains compatible with real-time measurements and local constraints. If the last schedule is no longer reliable or safe, the site switches to a conservative rule-based fallback policy, such as maintaining batteries within safe state-of-charge limits, prioritizing local load supply, limiting non-essential V2G discharge, avoiding avoidable peak imports or exports, and preserving user mobility, comfort, or process requirements. The platform and, where applicable, the local controller should log the event, including the reason for degradation, fallback strategy applied, affected assets, and restoration time. Once valid input data and communication are restored, the FlexBIT platform resumes rolling optimization and issues a new dispatch schedule.

At the Alu-Frost demonstrator, this strategy is implemented through an on-site sky-imaging pipeline jointly deployed by SRI PAS, WUST, and Electrum. An all-sky camera mounted on the building captures a hemispheric image every minute. Each new frame is passed to the image-based pipeline (Architecture A) running on the edge computer, which returns two forecasts — one for the next minute, one for 15 minutes ahead — together with sun elevation and azimuth computed from the timestamp. Both forecasts are written to the platform database, and a new dispatch schedule is generated on each cycle: the 1-minute value drives the immediate setpoint, while the 15-minute trajectory shapes what follows and reserves room for the irradiance changes coming next. This places Alu-Frost at the fast end of the cadence range noted earlier in this section — once per minute, against the 15 to 60 minutes typical of other sites. Every update is checked by the local controller against the current state of charge and ESS operating limits before any setpoint reaches the BESS through the EMACS interface.
If the camera goes offline or the image-based pipeline fails, the system falls back to Architecture B, the feature-based variant, which keeps producing forecasts at the same cadence from astronomical inputs and recent measurements. The dispatch loop continues without interruption. End-to-end latency — from frame capture to setpoint commit — has not yet been measured, since it depends on how quickly the image is rescaled, transmitted, and processed; this will be characterized during on-site commissioning. Both pipelines are retrained periodically on accumulated site data, and a fresh candidate is promoted to production only when it beats the incumbent on a held-out on-site test set.

7 Demonstrator Implementation (Per site)

7.1 Alufrost (Sowlany, Poland)

Overview asset	Industrial site with ESS (Energy Storage System), SCADA (EMACS), IoT sensors, energy meters, Edge computer + HPC backend (MLOps platform)	
Integration status	Gateway/Adapter	Edge computer as gateway
	Protocols	SCADA (EMACS), Delta Sharing API, Hadoop/Lakehouse integration
	Polling Rate	near real-time (seconds–minutes depending on signal)
Mechanisms implemented	REC	not implemented (industrial site)
	Flexibility	ESS charge/discharge optimization
	Balancing	local energy balancing (production vs consumption)
	Ancillary	potential support via ESS (future)
Control approach	Semi-autonomous control via EMACS SCADA + AI recommender (MLOps Digital Twin – ESS Estimator)	
Achievements	- ESS installed (Mesh4U) - SCADA integration - MLOps architecture defined	
Next steps	- ML model training (load, yield, price) - Full Digital Twin deployment - Optimization algorithms implementation	
Risks	- Data quality / availability - ML model accuracy - Integration complexity (Edge–HPC)	

7.2 Electrum Headquarter (Białystok, Poland)

Overview asset	Office building integrated with: • Building electrical infrastructure • Energy management and monitoring systems • SCADA (EMACS) platform • IoT devices and energy meters • Edge computing gateway • Digital Twin and MLOps components

Integration status	Gateway/Adapter	Industrial automation infrastructure integrated through Beckhoff PLC architecture with communication modules and Modbus-based data acquisition • Beckhoff PLC CX8180 • RS EL6021 communication modules • LE-03MW Modbus RTU modules • Energy analyzers
	Protocols	SCADA (EMACS), Modbus RTU, IoT interfaces, Delta Sharing API, and data integration toward Lakehouse / analytics environments.
	Polling Rate	near real-time (seconds–minutes depending on signal)
Mechanisms implemented	REC	Not implemented at building level; the demonstrator focuses on flexibility and internal optimization of energy use
	Flexibility	Demand-side flexibility through: • intelligent control of electrical loads, • consumption optimization, • adaptive scheduling of building energy usage, • support for future ESS integration.
	Balancing	Local balancing of building energy demand with operational conditions and consumption profiles.
	Ancillary	Potential future integration of flexibility services through ESS and aggregated demand response mechanisms
Control approach	Semi-autonomous operation combining: • EMACS SCADA supervision, • AI-based recommendation mechanisms, • Digital Twin representation of building behavior, • Edge-to-cloud data processing, • MLOps-enabled analytics for optimization and forecasting. Electrum positions EMACS as a platform supporting monitoring, optimization, and business-level analysis of energy assets.	
Achievements	• Deployment of monitoring and control infrastructure • Integration with EMACS SCADA platform • Establishment of edge computing architecture • Definition of Digital Twin and MLOps layers	

	• Demonstration environment prepared for flexibility use cases and optimization scenarios
Next steps	• Deployment of ML models for prediction and optimization • Full Digital Twin activation • Implementation of flexibility algorithms • Integration of advanced control strategies • Validation of building-level energy optimization scenarios
Risks	• Data quality and availability • Accuracy of optimization and forecasting models • Integration complexity between edge and cloud environments • Scalability toward additional demonstrator sites

7.3 WUST LAB (Wrocław, Poland)

Overview asset	Laboratory microgrid simulator including PV Array Simulator, AC Grid Simulator, PV inverter, BESS, controllable load, energy meters, power quality recorders, IT communication	
Integration status	Gateway/Adapter	Router, edge computer as gateway, microcomputer, PLC controller
	Protocols	Modbus, MQTT
	Polling Rate	near real-time (seconds–minutes)
Mechanisms implemented	REC	not implemented
	Flexibility	ESSS charge/discharge optimization, controllable load scheduling
	Balancing	local energy balancing (production vs consumption)
	Ancillary	potential support of grid, energy demand and reactive power via PV inverter and BESS
Control approach	Simplified data acquisition and control based on microcomputer and Node-RED application	
Achievements	- PV array simulator and AC Grid Simulator installed, -data acquisition integrated (energy meters, Modbus records) - regulatory potential tested (partially)	
Next steps	-integration with FlexBIT platform - semi autonomous control via microcomputer or PLC, expert based rules -identification of regulatory potential of BESS - identification of power quality impact	

Risks	- Integration complexity with FlexBIT platform (additional brokers, IT security issue)

7.4 UniTOV (Rome, Italy)

Overview asset	Laboratory renewable energy community simulator, including PV array, grid, BESS, controllable load, PEM fuel cell, metal hydrides hydrogen storage.	
Integration status	Gateway/Adapter	Raspberry Pi (or similar).
	Protocols	MQTT
	Polling Rate	Near real-time (minutes)
Mechanisms implemented	REC	Implemented (prosumers, local plant, consumers).
	Flexibility	BESS, hydrogen storage, demand-side management.
	Balancing	Local energy balancing (production-consumption) with the target of maximizing community self-consumption.
	Ancillary	Capacity reserve, peak shaving.
Control approach	- HiL demonstrator with remote controllers (both on a local and community level). - FlexBIT platform could communicate at a community level (with the central controller), or at a member level.	
Achievements	- Development of the full digital community. - Communication protocols within the demonstrator members.	
Next steps	- Hardware-in-the-Loop implementation. - Integration with FlexBIT platform.	
Risks	- Full demonstrator integration complexity. - Data exchange with FlexBIT platform.	

7.5 Arte Möbel (Magdeburg, Germany)

Overview asset	Industrial facility with a job-shop manufacturing process. Electricity is generated by PV modules, and various flexibility options are actively and passively controlled. Active flexibility options include an electrochemical energy storage system, a compressed air system, and an electric vehicle charging station. As a passive flexibility option, an energy management system sends visual notifications to machine operators, encouraging them to postpone or advance industrial processes according to the availability of PV-

	generated electricity. In addition to it, both the electric flows (generation and loads) as well as the material flows can be tracked by IoT devices.	
Integration status	Gateway/Adapter	Local PC -> Mosquitto -> IFF SCADA System
	Protocols	MQTT, MODBUS TCP, HTTP
	Polling Rate	near real-time (second–minute depending on signal)
Mechanisms implemented	REC	The demonstrator will focus both on operating as a Net-Zero Energy Factory and on participating in an industrial energy community. The German legal framework for Renewable Energy Communities (RECs) is considered to enable electricity sharing between aRTE Möbel and Aue Bestattungen.
	Flexibility	Battery, Compressed Air, EV Charger
	Balancing	On-site balancing will be implemented to operate the facility as a Net-Zero Energy Factory, while energy balancing between aRTE Möbel and Aue Bestattungen will support the sustainable production processes of aRTE Möbel through the sharing and optimal utilization of locally generated renewable electricity.
	Ancillary	Peak Shaving, Demand Response,
Control approach	- Gateway (PC) gets data from local devices - Data send via Mosquitto MQTT to IFF SCADA System and get processed - Control commands get calculated based on inbound timeseries and logic diagrams in IFF SCADA System - Control commands get send back to Demonstrator Gateway (PC) - Gateway sends control commands to local devices	
Achievements	- Data collection of local devices - Persistent data storage - Data Visualisation	
Next steps	- Control of devices	
Risks	- Inefficient Control logic - Equipment Failures - Poor Data quality / availability	

7.6 Aue Bestattungen (Magdeburg, Germany)

Overview asset	Tertiary facility in which electricity is generated by a PV plant. Flexibility is provided through an electrochemical energy storage system, two electric vehicle charging stations, and cooling units. The facility is operated to maximize the self-consumption of locally generated electricity and to support the sustainable manufacturing activities of aRTE Möbel through electricity sharing within an industrial energy community.	
Integration status	Gateway/Adapter	Local PC -> Mosquitto -> IFF SCADA System
	Protocols	MQTT, MODBUS TCP
	Polling Rate	near real-time (second–minute depending on signal)
Mechanisms implemented	REC	The demonstrator will focus both on operating as a Net-Zero Energy Facility and on participating in an industrial energy community. The German legal framework for Renewable Energy Communities (RECs) is considered to enable electricity sharing between aRTE Möbel and Aue Bestattungen
	Flexibility	Battery, Cooling aggregators, EV Charger
	Balancing	On-site balancing will be implemented to operate the facility as a Net-Zero Energy Facility, while energy balancing between aRTE Möbel and Aue Bestattungen will support the sustainable production processes of aRTE Möbel through the sharing and optimal utilization of locally generated renewable electricity.
	Ancillary	Peak Shaving, Demand Response
Control approach	- Gateway (PC) gets data from local devices - Data send via Mosquitto MQTT to IFF SCADA System and get processed - Control commands get calculated based on inbound timeseries and logic diagrams in IFF SCADA System - Control commands get send back to Demonstrator Gateway (PC) - Gateway sends control commands to local devices	
Achievements	- Data collection of local devices - Persistent data storage - Data Visualisation	
Next steps	- Control of devices	
Risks	- Inefficient Control logic - Equipment failures - Poor Data quality / availability	

7.7 Smart Energy Parking (Palermo, Italy)

Overview asset	Smart Parking lot within the Campus of the University of Palermo equipped with PV generator, stationary BESS, V1G and V2G charging stations and controllable lighting system	
Integration status	Gateway/Adapter	Local PC
	Protocols	HTTP, MODBUS TCP
	Polling Rate	near real-time (second–minute depending on signal)
Mechanisms implemented	REC	The demonstrator will focus on managing its own generation, storage and consumption for optimizing the energy exchanges and the total self-consumption in a REC context.
	Flexibility	Battery, Lighting system, EV Charger
	Balancing	On-site balancing will be implemented to operate the facility as a Net-Zero Energy Facility, while different control strategies can be implemented in order to exchange precise positive or negative power profile with the external grid.
	Ancillary	Peak Shaving, Demand Response
Control approach	- Gateway (PC) gets data from local devices - Data get processed - Control commands get calculated based on inbound timeseries and logic diagrams - Control commands get send back to Demonstrator Gateway (PC) - Gateway sends control commands to local devices	
Achievements	- Data collection of local devices - Persistent data storage - Data Visualisation	
Next steps	- Control of devices	
Risks	- Inefficient Control logic - Equipment failures - Poor Data quality / availability	

7.8 Solar Cooling System (Pantelleria, Italy)

Overview asset	The demonstrator is an innovative air-conditioning system (Freescoo 3.0 VMC) operating with low temperature heat (solar energy, heat pump, district heating, or waste heat) designed for controlled mechanical ventilation applications in the residential and tertiary sectors. The system is based on an

	original adsorption air treatment cycle capable of ensuring the control of air temperature and humidity, and guaranteeing adequate air exchange in the building. The system will be used to test the possibility of its use in load shifting actions by exploiting thermal inertia.	
Integration status	Gateway/Adapter	Local PC
	Protocols	HTTP, MODBUS TCP
	Polling Rate	near real-time (second–minute depending on signal)
Mechanisms implemented	REC	The demonstrator will focus on managing its consumption for a possible integration in a REC.
	Flexibility	Heat pump.
	Balancing	-
	Ancillary	Peak Shaving, Demand Response
Control approach	- Gateway (PC) gets data from local devices - Data get processed - Control commands get calculated based on inbound timeseries and logic diagrams - Control commands get send back to Demonstrator Gateway (PC) - Gateway sends control commands to local devices	
Achievements	- Data collection of local devices - Persistent data storage - Data Visualisation	
Next steps	- Control of devices	
Risks	- Inefficient Control logic - Equipment failures - Poor Data quality / availability - Connection issues	

8 References

[1] European Commission. “Energy communities.” European Commission, Directorate-General for Energy.
[2] European Commission. “Renewable Energy Directive.” European Commission, Directorate-General for Energy.
[3] European Commission. "Directive (EU) 2019/944 on common rules for the internal market for electricity." Official Journal of the European Union, 2019.
[4] European Commission Joint Research Centre. “Energy communities.” Smart Electricity Systems and Interoperability.
[5] NIST. Yaga, D., Mell, P., Roby, N., and Scarfone, K. “Blockchain Technology Overview.” NISTIR 8202, National Institute of Standards and Technology, 2018.
[6] Hyperledger Besu Documentation. “Configure QBFT consensus.” Hyperledger Besu.
[7] International Energy Agency (IEA), “Global ev outlook 2024,” tech.rep., International Energy Agency, Parigi, 2024. Accessed: 2025-05-21.
[8] European Commission, “Fit for 55: delivering the eu’s 2030 climate target on the way to climate neutrality.” https://commission.europa.eu/strategy-and-policy/priorities-2019-2024/european-green-deal/delivering-europes-digitaleconomy-and-green-transition\ en\#fit-for-55, 2021. Accessed: 2025-05-21.
[9] M. L. Di Silvestre, R. Musca, E. R. Sanseverino, G. Sciumè, A. Vasile, and G. Zizzo, “A feasibility study for the transition to electric mobility in the island of favignana,” in 2021 IEEE International Conference on Environment and Electrical Engineering and 2021 IEEE Industrial and Commercial Power Systems Europe (EEEIC / I&CPS Europe), 2021.
[10] G. Sciumè, C. Iurlaro, S. Bruno, R. Musca, P. Gallo, G. Zizzo, E. R. Sanseverino, and M. L. Scala, “A blockchain-based architecture for tracking and remunerating fast frequency response,” Sustainable Energy, Grids and Networks, vol. 40, p. 101530, 2024.
[11] B. Harish and U. Surendra, “A review on power quality issues in electric vehicle interfaced distribution system and mitigation techniques,” Indonesian Journal of Electrical Engineering and Computer Science, vol. 25, p. 656, 02 2022.
[12] B. Kamana-Williams, D. Bishop, G. Hooper, and J. Chase, “Driving change: Electric vehicle charging behavior and peak loading,” Renewable and Sustainable Energy Reviews, vol. 189, p. 113953, 2024.
[13] O. Sadeghian, A. Oshnoei, B. Mohammadi-ivatloo, V. Vahidinasab, and A. Anvari-Moghaddam, “A comprehensive review on electric vehicles smart charging: Solutions, strategies, technologies, and challenges,” Journal of Energy Storage, vol. 54, p. 105241, 2022.
[14] P. Barman, L. Dutta, S. Bordoloi, A. Kalita, P. Buragohain, S. Bharali, and B. Azzopardi, “Renewable energy integration with electric vehicle technology: A review of the existing smart charging approaches,” Renewable and Sustainable Energy Reviews, vol. 183, p. 113518, 2023.
[15] M. O. Dioha, T. H. Ruggles, S. Ashfaq, and K. Caldeira, “Idealized analysis of relative values of bidirectional versus unidirectional electric vehicle charging in deeply decarbonized electricity systems,” iScience, vol. 25, no. 9, p. 104906, 2022.
[16] Ministero dell’Ambiente e della Sicurezza Energetica (MASE), “Decreto Ministeriale del 07/12/2023, n. 414 sulle Comunità Energetiche Rinnovabili (in Italian),” 2023.
[17] M. L. D. Silvestre, F. Montana, E. R. Sanseverino, G. Sciumè, and G. Zizzo, “An algorithm for renewable energy communities designing by maximizing shared energy,” in 2023 AEIT International Annual Conference (AEIT), 2023.
[18] A. Dimovski, M. Moncecchi, and M. Merlo, “Impact of energy communities on the distribution network: An italian case study,” Sustainable Energy, Grids and Networks, vol. 35, p. 101148, 2023.
[19] G. Viganò, G. Lattanzio, and M. Rossi, “Review of main projects, characteristics and challenges in flexibility markets for services addressed to electricity distribution network,” Energies, vol. 17, no. 11, 2024.
[20] J. Barba, M. Canas-Carreton, M. Carrion, G. R. Hernandez-Labrado, C. Merino, J. I. Munoz, and R. Zarate-Minano, “Integrating hydrogen into power systems: A comprehensive review,” Sustainability, vol. 17, no. 13, 2025.
[21] C. Guille and G. Gross, “A conceptual framework for the vehicle-to-grid (v2g) implementation,” Energy Policy, vol. 37, no. 11, pp. 4379–4390, 2009.
[22] J. A. P. Lopes, F. Soares, and P. M. R. Almeida, “Integration of electric vehicles in the electric power system,” Proceedings of the IEEE, vol. 99, no. 1, pp. 168–183, 2011.
[23] I. Fernandez, T. San Roman, and R. Cossent, “Impact of smart charging and v2g on distribution grids with high pv penetration,” Electric Power Systems Research, vol. 184, p. 106309, 2020.
[24] K. Clement-Nyns, E. Haesen, and J. Driesen, “The impact of charging plug-in hybrid electric vehicles on a residential distribution grid,” IEEE Transactions on Power Systems, vol. 25, no. 1, pp. 371–380, 2010.
[25] T. Morstyn, N. Farrell, S. J. Darby, and M. D. McCulloch, “Using peer-to-peer energy-trading platforms to incentivize prosumers to form federated power plants,” Nature Energy, vol. 3, no. 2, pp. 94–101, 2018.
[26] A. Y. Saber and G. K. Venayagamoorthy, “Resource scheduling under unRECtainty in a smart grid with renewables and plug-in vehicles,” IEEE Systems Journal, vol. 6, no. 1, pp. 103–109, 2012.
[27] L. Yao, W. H. Lim, and T. P. Tsai, “A real-time charge scheduling algorithm for demand response in electric vehicle charging stations,” IEEE Transactions on Smart Grid, vol. 8, no. 1, pp. 52–62, 2013.
[28] Parker Project Consortium, “Parker project: Final report.” Technical Report, 2019. https://parker-project.com.
[29] Electric Nation Project Consortium, “Electric nation: Learnings from the uk’s largest ev trial.” Technical Report, 2019. https://www.electricnation. org.uk.
[30] S. Ramos, A. Chiodi, and et al., “Local energy communities with electric vehicles: Assessing v2g and smart charging in a residential district,”Applied Energy, vol. 292, p. 116883, 2021.
[31] Gestore dei Servizi Energetici (GSE), “Comunità di energia rinnovabile e gruppi di autoconsumatori: pubblicati i profili standard per prelievo e immissione 2025,” 2024. Accessed: 2025-04-07.
[32] European Commission, Joint Research Centre, “Photovoltaic Geographical Information System (PVGIS),” 2025. Accessed: 2025-04-07.

[33] Sharma, V.; Haque, M.H.; Aziz, S.M.; Kauschke, T. Smart Inverter and Battery Storage Controls to Reduce Financial Loss Due to Overvoltage-Induced PV Curtailment in Distribution Feeders. Sustain. Energy, Grids Networks **2023**, 34, 101030, doi:10.1016/j.segan.2023.101030.
[34] Micheli, L.; Soria-Moya, A.; Talavera, D.L.; Abbasi, B.; Fernández, E.F. Energy and Economic Implications of Photovoltaic Curtailment: Current Status and Future Scenarios. Sustain. Energy Technol. Assessments 2025, 81, doi:10.1016/j.seta.2025.104414.
[35] F. Olivier, P. Aristidou, D. Ernst, and T. Van Cutsem, "Active Management of Low-Voltage Networks for Mitigating Overvoltages Due to Photovoltaic Units," IEEE Trans Smart Grid, vol. 7, no. 2, pp. 926–936, Mar. 2016, doi: 10.1109/TSG.2015.2410171.
[36] H.-J. Lee, K.-H. Yoon, J.-W. Shin, J.-C. Kim, and S.-M. Cho, "Optimal Parameters of Volt–Var Function in Smart Inverters for Improving System Performance," Energies (Basel), vol. 13, no. 9, p. 2294, May 2020, doi: 10.3390/en13092294.
[37] R. Tonkoski, L. A. C. Lopes, and T. H. M. El-Fouly, "Coordinated Active Power Curtailment of Grid Connected PV Inverters for Overvoltage Prevention," IEEE Trans Sustain Energy, vol. 2, no. 2, pp. 139–147, Apr. 2011, doi: 10.1109/TSTE.2010.2098483.
[38] R. K. Gupta and D. K. Molzahn, "Improving fairness in photovoltaic curtailment via feedback-driven daily topology reconfiguration in power distribution networks," Appl Energy, vol. 400, p. 126543, Dec. 2025, doi: 10.1016/j.apenergy.2025.126543.
[39] F. M. Camilo, R. Castro, M. E. Almeida, and V. Fernão Pires, "Assessment of overvoltage mitigation techniques in low-voltage distribution networks with high penetration of photovoltaic microgeneration," IET Renewable Power Generation, vol. 12, no. 6, pp. 649–656, Apr. 2018, doi: 10.1049/iet-rpg.2017.0482.